nature reviews earth & environment

https://doi.org/10.1038/s43017-022-00364-y

Review article

Check for updates

Diversity of magmatism, hydrothermal processes and microbial interactions at mid-ocean ridges

Gretchen L. Früh-Green[1] ✉, Deborah S. Kelley[2], Marvin D. Lilley[2], Mathilde Cannat[3], Valérie Chavagnac[4] & John A. Baross[2]

Abstract

Hydrothermal circulation and alteration at mid-ocean ridges and ridge flanks have a key role in regulating seawater chemistry and global chemical fluxes, and support diverse ecosystems in the absence of light. In this Review, we outline tectonic, magmatic and hydrothermal processes that govern crustal architecture, alteration and biogeochemical cycles along mid-ocean ridges with different spreading rates. In general, hydrothermal systems vary from those that are magmatic-dominated with low-pH fluids >300 °C to serpentinizing systems with alkaline fluids <120 °C. Typically, slow-spreading ridges (rates <40 mm yr^{-1}) have greater variability in magmatism, lithology and vent chemistry, which are influenced by detachment faults that expose lower-crustal and serpentinized mantle rocks. Hydrothermal alteration is an important sink for magnesium, sodium, sulfate and bicarbonate, and a net source of volatiles, iron and other nutrients to the deep ocean and vent ecosystems. Magmatic hydrothermal systems sustain a vast, hot and diverse microbial biosphere that represents a deep organic carbon source to ocean carbon budgets. In contrast, high-pH serpentinizing hydrothermal systems harbour a more limited microbial community consisting primarily of methane-metabolizing archaea. Continued advances in monitoring and analytical capabilities coupled with developments in metagenomic technologies will guide future investigations and discoveries in hydrothermal systems.

Sections

A full list of affiliations appears at the end of the paper. ✉e-mail: frueh@ethz.ch

Key points

- Spreading rates control variations in heat sources, magma input and tectonic processes along mid-ocean ridges and influence crustal architecture and hydrothermal processes, providing multifaceted habitats for life.

- Approximately one-third (7×10^{12} to 11×10^{12} W) of the global oceanic heat flux (32×10^{12} W) occurs through hydrothermal convection at ridges and ridge flanks. Seawater circulation, hydrothermal alteration and microbial interactions regulate seawater chemistry and change the composition and physical properties of the lithosphere.

- Roughly 50% of the global mid-ocean ridges are spreading at rates <40 mm yr^{-1}, where major detachment faults expose lower-crustal and upper-mantle rocks, creating asymmetric ridge segments with large variability in structure, hydrothermal processes and vent fluid chemistry.

- Serpentinization decreases bulk density (<2.9 g cm^{-3}) and seismic velocities (V_p < 6 km s^{-1}) of mantle rocks and weakens the oceanic lithosphere along detachment faults. Serpentinization reactions produce highly reduced fluids with high H_2, CH_4 and other organic molecules that provide energy for microbial life.

- Hydrothermal processes govern global chemical fluxes (such as Mg, Fe, Mn and volatiles) and provide nutrients (for example, Fe flux ~$4–6\times10^{9}$ mol yr^{-1}) to the deep ocean. Approximately 0.05 GtC yr^{-1} of organic carbon is estimated to be produced through microbial interactions and oxidation of organic compounds within hydrothermal plumes.

- Basalt-hosted systems support a vast, hot and diverse microbial biosphere, in contrast to serpentinizing systems, which sustain more limited microbial communities primarily dominated by methane-metabolizing archaea. Advanced technologies allow better characterization of the genetic makeup and metabolism of microbes and the role of viruses in shaping diversity.

Introduction

Mid-ocean ridge (MOR) systems extend approximately 60,000 km around the globe and are the most dynamic and continuous tectonic feature on the planet (Fig. 1). On average, about 3.3 km^2 yr^{-1} of new oceanic crust is generated at global spreading centres[1], which account for >70% of the total volcanism, and where about 60–70% of the Earth's surface has been produced over the past 160–180 Myr (ref.[2]). Mantle melting, volcanism and faulting at MORs drive hydrothermal circulation that allows the transfer of heat, chemical compounds, metals and volatiles from the asthenosphere to the hydrosphere and biosphere. Approximately 75–80% of the Earth's total heat flux occurs as the oceanic crust ages[3–5], and it is most pronounced at ridge flanks[6], where low-temperature fluid flow continues off axis for millions of years and contributes to global biogeochemical cycles[4,7]. It is estimated that the volume of the ocean circulates through the oceanic ridge system in much less than 1 Myr (ref.[6]).

Spreading centres are one of the most extreme environments on Earth that can support oases of life at high temperatures and thriving in perpetual darkness. Microorganisms obtain energy from magmatic gases and chemical compounds of altered oceanic crust, rather than from light, through a process called chemosynthesis[8–10]. In turn, many of these microorganisms symbiotically sustain macrofaunal communities that populate hydrothermal vent environments[8]. The microorganisms with the highest known growth temperature on Earth are found within MOR hydrothermal systems[11,12], and investigation of their genetic diversity has changed the current view of the tree of life[13,14].

Only a small percentage of the global seafloor has been investigated, and as such, the deep ocean remains one of the last frontiers on Earth to be explored and directly sampled. Diffuse, low-temperature (6–17 °C) hydrothermal vents were first discovered in 1977 at the Galápagos Spreading Centre in the equatorial Pacific[10]. In early 1979, high-temperature (>350 °C), low-pH fluids discharging from sulfide structures were found on the East Pacific Rise (EPR) at 21° N (ref.[15]) and demonstrated for the first time that seafloor hydrothermal fluids could transport high concentrations of ore-forming elements[16]. Diffuse springs associated with these vents were found to support exotic benthic communities of giant tubeworms, clams and crabs similar to those found at the Galápagos Ridge, which survive through symbiotic relationships with bacteria that oxidize reduced sulfur[17]. These exciting discoveries inspired subsequent multidisciplinary research into MOR systems that brought to light the complex interplay of magmatism, tectonics, hydrothermal circulation and fluid–rock interaction linked to seawater chemistry and life.

Since the first discoveries, more than 500 sites of hydrothermal venting on the seafloor have been identified[18] (Fig. 1). Integrated approaches of targeted drilling, sampling, biogeochemical analyses, seismic experiments, modelling and real-time observations at ocean observatories (Box 1) are providing fundamental insights about Earth and the evolution of life, and offer unlimited opportunities for new discoveries. In addition to the pivotal discoveries in the late 1970s of exotic ecosystems around hydrothermal vents[8,19], advances have been made in monitoring earthquakes and volcanic eruptions in real time and in understanding the extent of the subsurface biosphere. Advanced analytical and microbiological techniques are helping to constrain the role of submarine volcanoes in controlling ocean chemistry and give insights into novel lifeforms, their metabolic and genetic diversity, and evolution.

This Review provides an overview of tectonic, magmatic and hydrothermal processes that govern variations in crustal architecture, water–rock–microorganism interactions and hydrothermal fluxes in MOR systems. We summarize key differences among ridges with differing spreading rates that have experienced varying degrees of magmatism and tectonism. This Review is not intended as a comprehensive compilation of all major sites. Instead, we focus on a few well-studied examples from the EPR, Juan de Fuca Ridge (JdF) and Mid-Atlantic Ridge (MAR), highlighting variations in geological and biogeochemical processes that result in a diversity of hydrothermal environments and associated ecosystems.

Variations in MOR spreading

A wide range of geological features form at ocean rifts as lithospheric plates diverge and new crust is created (Fig. 2). The morphology and oceanic crustal architecture of MORs, and the hydrothermal systems they host, are governed by differences in magmatic, tectonic and alteration processes, which are directly a function of spreading rates and vary in response to regional tectonic stresses and magma supply. These magmatic and tectonic variations at MORs are discussed in this section alongside how they are monitored.

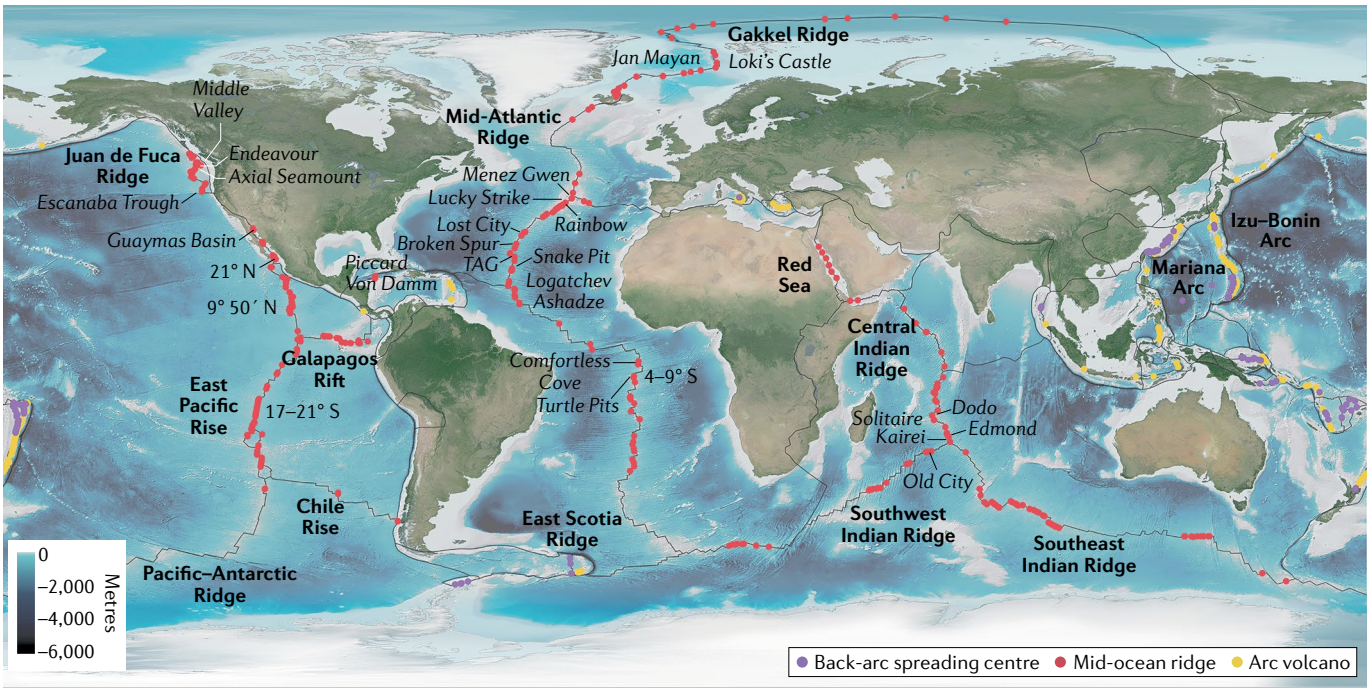

Fig. 1 | Global distribution of hydrothermal vents on the seafloor. Map of the global ridge system with distribution of known sites of hydrothermal venting and sites inferred to be present from water-column studies. Hydrothermal vents occur at MORs (65% of known sites), back-arc spreading centres (22%), submarine arc volcanoes (12%) and interplate hot spot volcanoes (1%) (ref.[148]). Data from the InterRidge Vents Database. Map adapted with permission from the Center for Environmental Visualization, University of Washington.

Fast-spreading ridges

Fast- and ultrafast-spreading ridges (>80 mm yr^{-1}) generally have high magmatic budgets and erupt voluminous basaltic lavas that accommodate extension, forming a smooth central raised axial ridge with little faulting. The EPR (Fig. 1) is the fastest-spreading MOR, currently reaching rates >100 mm yr^{-1} near 10° N and 150 mm yr^{-1} near 30° S (refs.[20,21]). Regions with a continuous input of magma are thought to result in a relatively uniform, layered crustal structure, with volcanic and plutonic rocks that are similar to lithostratigraphy found in some ophiolites (such as in Cyprus and Oman). Typically, this general layer-cake stratigraphy, referred to as Penrose-type crust[22], consists of a sequence of pillow basalt and lava flows, sheeted dykes, and gabbros that commonly contain ultramafic cumulates, overlying variably tectonized upper-mantle sequences (Fig. 2a).

Most conceptual models of fast-spreading ridges are based on geophysical studies of the EPR. These models predict that sub-Moho melts feed sills through small dykes and accumulate in a shallow axial melt lens (AML), 1–2 km beneath the ridge axis[23,24] (Fig. 2a). There are contrasting conceptual models for the formation of the gabbroic lower crust at fast-spreading ridges that predict differences in lower-crustal structure and have different implications for thermal and magnetic properties and hydrothermal cooling. Two leading models invoke either crystallization of multiple stacked magmatic sills (referred to as the sheeted sill model; Fig. 2a); or the presence of a small sill at the base of the sheeted dyke complex from which gabbro cumulates crystallize and subside to form the lower crust (referred to as the gabbro glacier model; see review in ref.[25]).

Sheeted sill models predict an axial heat flux of ~15 MW km^{-1} and require extensive, fast hydrothermal cooling along a mush zone to remove latent heat of crystallization at the ridge axis[25]. In contrast, gabbro glacier models predict that most crystallization occurs within the shallow magma sill, with slow cooling and higher axial heat fluxes of ~30 MW km^{-1} through hydrothermal circulation[25]. Microstructural, crystallographic and petrological data from the lower crust at Pito Deep on the EPR[26,27] support both models and document regional and temporal variations in crystallization, magmatic flow and faulting with depth in the gabbroic sequences but at relatively constant and fast spreading rates[26]. The magnetic structure preserved at Pito Deep also suggests that crustal temperatures remained around 500 °C up to ~8 km off axis[27]. The continuous release of latent heat over this broad region would delay the onset of conductive cooling in the lower crust.

High-temperature hydrothermal vents at the EPR are fuelled by small, shallow magma chambers (Fig. 2a) and are influenced by frequent volcanic eruptions that occur every 10–20 years (see overview in ref.[28]). Frequent eruptions can bury young vents and biological communities and result in smaller sulfide structures and fewer vents along the ridge axis. Eruptive fissures and margins of the EPR axial graben provide well-established permeable pathways for hot fluids to ascend through the crust[28]. The EPR 9° 50′ N area was the first documentation of a seafloor eruption in 1991 and of the impact it can have on both vent fluid chemistry and the surrounding water column[29,30]. For example, time-series analyses of vent fluids sampled within a month of the 1991 eruption documented changes in chloride contents, which were dominated by a vapour phase directly after the eruption but showed an increase in chlorinity to greater than seawater values in 3 years or less[31]. Prediction of a repeat eruption in the same area and observation of the microearthquake character of the eruption was recorded by

Box 1

Ocean observatories

Ocean-floor observatories have advanced the ability to study interactions of seafloor deformation, volcanism, hydrothermal circulation and microbial activity during ocean crust evolution. Below, we provide a brief overview of three ocean observatories currently installed to study MOR processes.

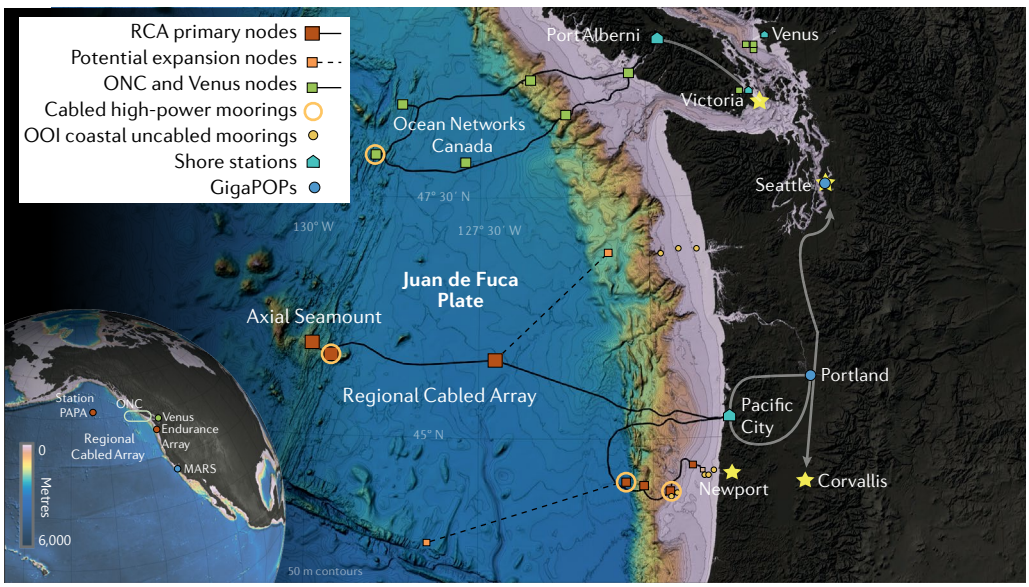

Regional Cabled Array (RCA) and Ocean Networks Canada (ONC): combined, these two instrumented networks on the Juan de Fuca Ridge form the first submarine cabled observatories to monitor an entire tectonic plate. The mid-ocean ridge components of the two observatories focus on both the magmatically robust Axial Seamount (RCA as part of the Ocean Observatories Initiative (OOI), operated by the United States), which erupted in 1998, 2011 and 2015, and the tectonically active Endeavour Segment (ONC, operated by Canada)[231,240] (see figure). These two networks are linked to the global Internet and provide data and imagery in real- to near-real time. Continuous monitoring of the oceanic plate is made possible through ~1,700 km of fibre optic cable and 14 subsea terminals that provide 8–10 kW power and 10 Gbs two-way communications to hundreds of instruments on the seafloor and in the water column. A highlight of the networked RCA was the live detection of the 2015 Axial Seamount eruption, marked by a seismic crisis of >8,000 earthquakes coincident with 2.4 m of seafloor subsidence over a 24-hour period[241]. Hydrophones detected acoustic activity delineating more than 30,000 volcanic explosions as lava spilled onto the seafloor[242], culminating in a 127-m-thick submarine lava flow. Three months later, the summit of the flow was covered by kilometres of microbial mats fed by nutrient-rich warm fluids circulating through the cooling lava[119].

European Multidisciplinary Seafloor and water-column Observatory (EMSO) is located on the Mid-Atlantic Ridge south of the Azores. The principal target of the uncabled EMSO is to understand shorter-term variations of the Lucky Strike hydrothermal system in a tectonically complex framework, and their impact on life at and beneath the seafloor, similar to the JdF sites. One observatory node of the EMSO infrastructure is dedicated to long-term (>20 years) monitoring of volcanic, tectonic, hydrothermal and biological activity at Lucky Strike[67]. The observatory includes arrays of autonomous instruments and two stations that communicate acoustically to a surface-relay buoy which transmits data to shore every 6 hours. Two stations monitor seismic activity, pressure at the seafloor and key environmental parameters; one of these stations also connects to a camera that records daily videos of the hydrothermal fauna. Monitoring of variable responses to tidal forcing has revealed changes in the subseafloor permeability structure[243,244] and episodic increases in microseismic activity. Changes in earthquake locations through time indicate that the main heat extraction is to the north of the hydrothermal field and moved by about 800 m to the east between late 2013 and late 2015[245]. GigaPOPs, Gigabit point of presence; MARS, Monterey Accelerated Research System. Map adapted with permission from the Center for Environmental Visualization, University of Washington.

ocean-bottom seismometers in mid-2005 and documented an intense but brief inferred dyking event in early 2006[32,33]. Seismic monitoring at the 9° 50′ N area between 2003 and 2004 also provided a regional picture of the distribution of tectonic and hydrothermal stresses that control permeability and promote along-axis flow above the axial magma chamber[34].

Intermediate-spreading ridges

Mid-ocean ridges with intermediate spreading rates (40–80 mm yr^{-1}) exhibit transitional morphologies, crustal structure and variations in hydrothermal output. Temporal and spatial variations in magmatism along these ridges result in both magma-rich regions around axial highs and magma-poor regions more influenced by faulting. The

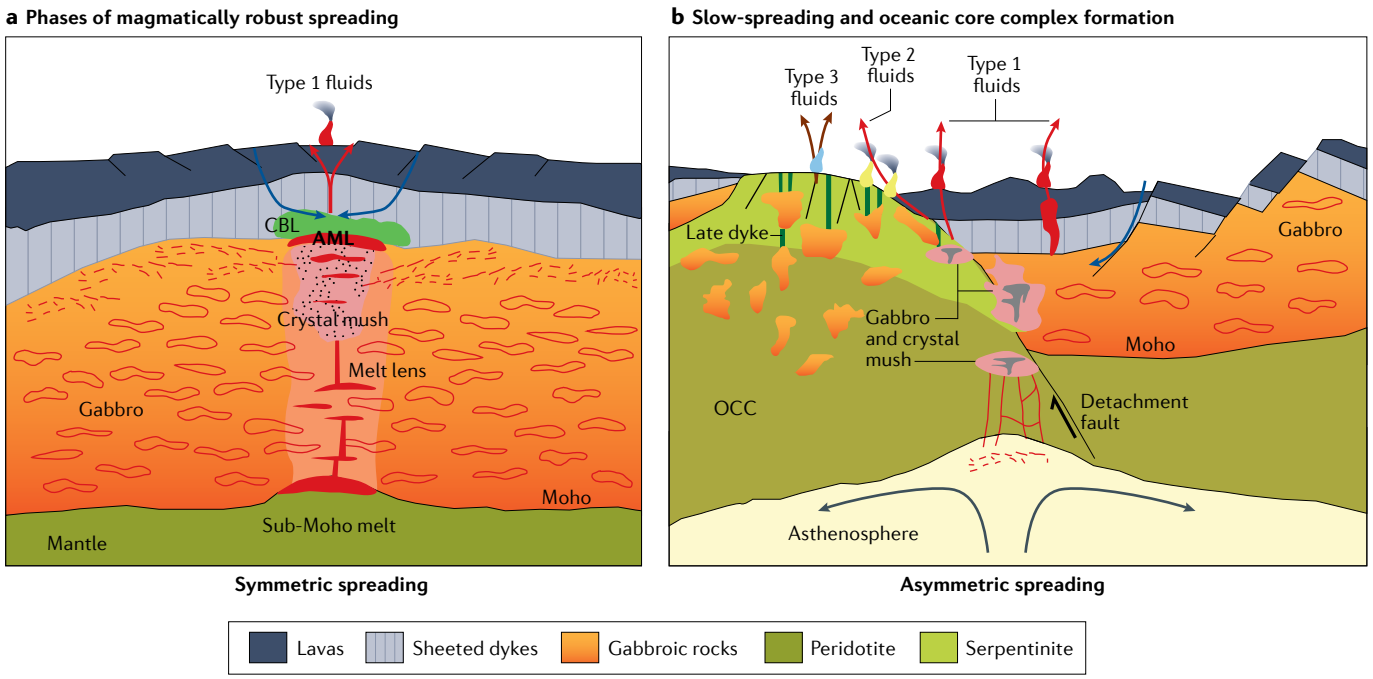

c Types of hydrothermal vent systems

Type 1 fluids

High-temperature vents with sulfide deposits in basalt

- $T > 300$ °C
- Low pH (<5)
- High metals
- High CO_2, variable H_2S
- Low but variable H_2, CH_4
- Abundant macrofauna

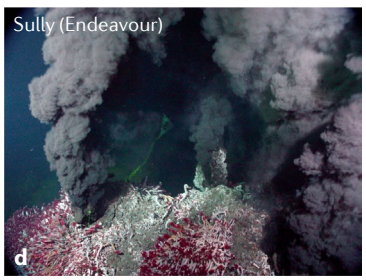

Type 2 fluids

High-temperature vents with sulfide deposits in serpentinites and gabbro

- $T > 300$ °C
- Low pH (<5)
- High metals
- High CO_2 (gabbroic input)
- High H_2, CH_4 (ultramafic input)
- Abundant macrofauna

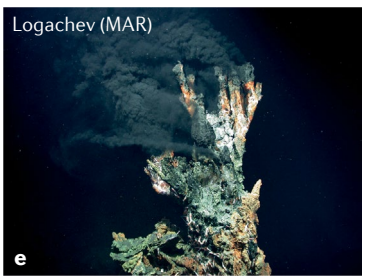

Type 3 fluids

Low-temperature vents with carbonate deposits in serpentinite

- $T < 120$ °C
- High pH (>9)
- Low metals
- Negligible CO_2
- High abiogenic H_2, CH_4, formate
- Limited macrofauna, diverse meiofauna

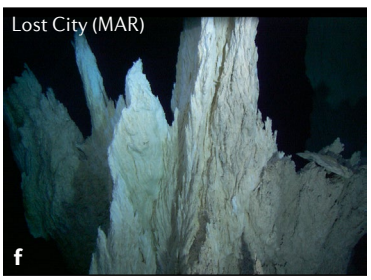

Fig. 2 | Variations in magmatism, structure and hydrothermal systems with varying spreading rates. Conceptual, across-axis comparison with variations in magmatism and spreading rate. **a**, Regions with phases of robust magmatism, characteristic of fast-spreading MORs, produce a relatively homogeneous layered crust. Current geophysical models predict that sub-Moho melts feed sills through small dykes and accumulate in a shallow axial melt lens (AML), producing stacked sills and a crystal mush zone (high melt %; stippled region) surrounded by hot gabbroic rock[23]. A conductive boundary layer (CBL) separates the AML from hydrothermal circulation where focused fluid flow produces high-temperature type 1 vent fields. Depth of profile ~6 km. **b**, Slow-spreading ridges are heterogeneous and influenced by discontinuous magmatism leading to detachment faults, asymmetric ridge segments and oceanic core complexes (OCC). Detachment faults can channel high-temperature type 1 fluids (such as at Trans-Atlantic Geotraverse field[63,76,148]) and drive flow in gabbro- and peridotite-influenced type 2 hydrothermal systems (such as at Logatchev and Rainbow[139,140,234]). Late normal faults can focus low-temperature, alkaline fluids (type 3 fluids) leading to large carbonate deposits, as at Lost City[65,80]. Depth of profile ~9 km. **c**, Types of hydrothermal vents described in panels **a** and **b**. **d**, The structure named Sully on the Endeavour Segment, Juan de Fuca Ridge, overgrown with *Ridgeia piscesae* tubeworms venting 380 °C type 1 black smoker fluids after a dyking event in 1999–2000. **e**, The black smoker structure named Candelabra, venting type 2 fluids at a water depth of 3,300 metres in the Logatchev hydrothermal field, MAR. **f**, Carbonate–brucite deposits at 845 m water depth at the Lost City hydrothermal field, MAR 30° N; see also Supplementary Movies 3 and 4. Panel **a** adapted with permission from ref.[23], Wiley. Panel **b** adapted with permission from ref.[235], Mineralogical Society of America. Panel **d** courtesy of University of Washington, NSF-OOI, CSSF. Panel **e** reprinted from MARUM, CC BY 4.0 (https://creativecommons.org/licenses/by/4.0/). Panel **f** courtesy of IFE, URI-JAO, Lost City Science Party and NOAA Ocean Exploration.

best-studied examples are the JdF and Gorda Ridge system (900 km in length) and the Galapagos Rift (1,700 km in length). Seismic imaging of the JdF indicates stacked subaxial magma lenses at depths of ~1.7–4.5 km, extending ~1–8 km along axis, which underlie the majority of high-temperature vent sites[23].

Axial Seamount on the JdF is the most magmatically active submarine volcano in the northeast Pacific (Supplementary Movie 1), where an extensive cabled network of multidisciplinary instruments has been installed and dedicated for 25 years of operation (Regional Cabled Array; Box 1). It was the first site where stacked magmatic sills were imaged and where the full evolution of an eruption in real time was captured[35–37]. Long-term measurements of summit inflation and deflation before and after seafloor eruptions at Axial led to the first forecasting model for a submarine eruption[38,39].

The Endeavour Segment of the JdF (Supplementary Movie 2) is one of the most vigorously active hydrothermal areas on the global MOR system and has been the subject of numerous multidisciplinary research efforts since the early 1980s[40–44]. Similar to Axial, it is monitored by a cabled array of instruments, implemented by Ocean Networks Canada (Box 1). Unlike Axial, no historical seafloor eruptions have been detected at Endeavour. However, widespread venting has produced abundant large sulfide chimneys, some of which are the largest sulfide structures ever discovered[44,45].

Slow- and ultraslow-spreading ridges

Roughly 50–60% of the global ridge system is spreading at rates <40 mm yr^{-1}, and includes the MORs that extend from the Arctic Ocean, along the entire Atlantic Ocean, and into the Indian Ocean[46,47]. Slow-spreading (20–40 mm yr^{-1}) and ultraslow-spreading (<20 mm yr^{-1}) ridges have rugged topographies and a large variability in exposed and subsurface rock types, magma supply and tectonic extension. Plate separation is partly accommodated by faulting, resulting in asymmetric axial valleys and large-offset normal faults, called oceanic detachment faults, similar to structures in continental extensional settings[48] (Fig. 2b). In these environments, the interplay of discontinuous magma supply and tectonic processes results in highly heterogeneous oceanic lithosphere and exposure of lower-crustal and upper-mantle rocks, leading to major variations in geophysical properties, structure and geochemistry along and across ridge axes.

Oceanic detachment faults are recognized as a distinct mode of oceanic accretion and have a key role in fluid circulation[49]. Serpentinized mantle peridotite and lower-crustal plutonic rocks exposed through detachment faults represent on average 25% of the seafloor[47,50]. Long-lived (>1 million years) detachment systems result in dome-shaped massifs, with spreading-parallel undulations (corrugations) of the seafloor. These corrugated domes, termed oceanic core complexes (OCCs) or megamullions[51,52], are common along the Mid-Atlantic and Southwest Indian Ridges (SWIR)[53–55]. OCCs form in the footwall of axial detachments during periods of reduced and variable magma supply and are juxtaposed to more volcanic seafloor in the opposite plate[56,57] (Fig. 2b). In some ultraslow-spreading locations, such as the easternmost SWIR and regions of the Gakkel Ridge in the Arctic[56,58,59], very low melt supply results in more extensive, widespread exposures of mantle rocks[56]. Studies of OCCs have documented complex histories of deformation[54,60–62] and fluid circulation[63,64] along the detachment fault zones leading to active hydrothermal systems, such as the high-temperature TAG (Trans-Atlantic Geotraverse)[69,72] and the serpentinite-hosted Lost City hydrothermal fields[65,66].

The northern MAR is the best-studied slow-spreading environment and currently the site of an uncabled seafloor and water-column observatory dedicated to long-term (>20 years) monitoring of volcanic, tectonic, hydrothermal and biological activity at the basalt-hosted Lucky Strike hydrothermal field[67] (Box 1). Measurements at Lucky Strike have revealed an estimated minimum total heat flux of 200 MW (refs.[68,69]), similar to heat flux estimated at the Costa Rica Rift[70]. Numerical modelling predicts along-axis hydrothermal flow at Lucky Strike[71], which is consistent with more recent seismic studies at 9° 50′ N on the EPR[34].

Multidisciplinary investigations of MORs continue to provide a better understanding of variations in seafloor spreading processes as a function of spreading rate and highlight the complex relationship between magmatic and tectonic processes that influence the formation of volcanic and plutonic crust and exposure of mantle rocks on the seafloor. Differences in magmatic activity and crustal architecture also control seawater circulation, hydrothermal alteration and vent fluid chemistry, which affect hydrothermal fluxes and microbial interactions, and are discussed in the following sections.

MOR hydrothermal systems

Contrary to early assumptions, hydrothermal circulation in the oceanic crust and the distribution and composition of MOR vents are highly variable, and depend on the interplay of tectonic, magmatic, geochemical and biological processes.

Hydrothermal circulation at MORs

Penetration of seawater is limited in all settings to the depth of the brittle lithosphere, which is a function of spreading rate and thermal structure. Permeability in this brittle domain probably decreases with depth, and hydrothermal circulation is expected to be restricted to <6 km, with the possible exception of the damage zone of axial detachment faults[72]. At fast-spreading ridges, axial magma chambers at depths of 1–2 km drive shallow hydrothermal circulation[24,73,74]. Models of the thermal structure of MORs that fit multichannel seismic data and axial earthquake centroid depths[75] suggest that a steady-state magma lens can only exist at depths <6 km at spreading rates greater than ~40–60 mm yr^{-1}. As spreading rates decrease, persistent magma bodies are deeper and the permeability of the upper lithosphere becomes more complex, with fluids channelled along normal faults that can reach 5–8 km into the oceanic lithosphere[76]. Therefore, at slower-spreading ridges, only transient melt bodies can exist at depth[77,78] and hydrothermal circulation mainly occurs along faults. In the following section, the main types of hydrothermal systems are discussed, but we emphasize that a strict categorization of vent types is not always applicable.

Types of hydrothermal systems

The type of rocks in the subsurface of hydrothermal systems together with variability in heat sources and faulting have a profound influence on fluid circulation pathways, vent distribution and fluid chemistry. At least three general classes of vent systems have been distinguished[79] (Fig. 2): high-temperature (>300 °C) hydrothermal systems driven by cooling magmas and/or proximal gabbroic crust; high-temperature hydrothermal vents (>300 °C) in detachment settings where variable mixtures of gabbro and peridotite influence heat and mass fluxes; and low- to moderate-temperature (less than ~120 °C) hydrothermal activity driven by cooling of mantle-dominated lithosphere resulting in serpentinization, alkaline fluids and precipitation of carbonate chimneys, exemplified by Lost City[65,80] on the MAR and Old City on the SWIR[81] (Fig. 2f).

However, not all MOR hydrothermal systems fit directly into these general categories. For example, the ultraslow Mid-Cayman spreading centre in the Caribbean Sea is the deepest site yet discovered that has multiple hydrothermal vents and likely different sources, all in close

proximity at varying water depths[82]. At Mid-Cayman, the vent fluid chemistry and temperatures are intermediate between high- and low-temperature systems[82–84] (Supplementary Data). The most prominent feature is Mount Dent, a topographic high on the western flank of the axial valley, which hosts multiple vent fields with abundant fauna, including the Von Damm and Piccard vent fields at depths of 2,300 m and 4,960 m, respectively[82]. Mount Dent is interpreted as an OCC, and the fluid geochemistry reflects the influence of both gabbroic and ultramafic rocks along the flow and alteration pathways[85]. In contrast to other high-temperature systems, hydrothermal activity at the Von Damm vent field, with fluid temperatures up to 226 °C, could be supported by deep fissuring on the OCC, allowing heat to be mined from a deep crustal source rather than from cooling of magma at depth[82].

The diversity of hydrothermal systems at MORs reflects variations in heat sources and differences in subsurface rock types. In general, magmatism fuels high-temperature hydrothermal systems with variable chemistry that are found in all spreading environments, whereas deep faulting promotes lithospheric cooling and drives medium- to low-temperature systems with fluid compositions indicative of interaction with lower-crustal and upper-mantle rocks exposed on, or close to, the seafloor.

Vent distribution and chemistry

Sampling and measurements over multiple months and years provide important constraints on regional and temporal variations in seismic activity, hydrothermal circulation, permeability, fluid–rock and microbiological interactions, and how these are affected by tectonic and magmatic events[31,40,86]. The key controls on the distribution of hydrothermal systems and their vent chemistry are discussed in the following sections (Fig. 3).

Alteration along convection pathways

As seawater-derived fluids penetrate the crust and are heated at depth, convection cells are established, resulting in zones of hydrothermal upflow and fluid discharge onto the seafloor that drive cold seawater downflow and recharge of the system (Fig. 3b). Water–rock reactions along the convection pathway result in chemical exchange that alters the composition of the host rocks and transforms seawater into hydrothermal fluids.

Basalt-hosted and high-temperature systems. The highest-temperature and deepest portion of the hydrothermal circulation cell is known as the reaction or root zone[87], although reactions occur over the entire circulation pathway and continue on the ridge flanks. Hydrothermal alteration of the oceanic lithosphere at varying temperatures is an important sink for seawater-derived Mg, sulfate and alkali elements (Fig. 3b), but a source for many others, such as Ca, Cu, Fe, Mn, Zn, Pb, Li, Rb, REE and Cs[31,87]. Volatiles, such as H_2, CO_2, H_2S and CH_4, can be released through magmatic degassing or form through fluid–rock reactions and can be used or produced by microbial ecosystems at and beneath the seafloor[9,42]. At the deepest level of penetration in magmatic systems, water–rock reactions produce greenschist-facies minerals in the reaction zone and acidic hydrothermal fluids, which are enriched in metals and volatiles and are extremely hot: 350 °C to >400 °C (Supplementary Data). High-temperature fluids are buoyant and rapidly rise to the seafloor through pipe-like conduits. Mixing of superheated fluids with cold seawater at and near the seafloor causes dissolved metals to precipitate and leads to the formation of variably sized edifices and sulfide deposits forming black and (less commonly) white smoker chimneys that have become hallmarks for hot marine hydrothermal systems[28,88] (Fig. 3b).

Diffuse fluid flow at hydrothermal vents. There are two types of low-temperature or 'diffuse' vents that are integral components of magma-driven hydrothermal environments. One type of diffuse venting occurs in basalts that are too fractured for the flow path to become sealed (as in high-temperature vents), and the rising hot fluid mixes with seawater to produce dispersed fluids with temperatures of 5 °C to ~50 °C (Fig. 3b, orange arrows). Geochemical data indicate that such diffuse fluids show a loss of H_2S and H_2 and gain of CH_4 that are not simply dilutions of high-temperature vent fluids but point to subsurface microbial interactions[89,90]. The microbial populations associated with such diffuse sites can be spatially distinct but temporally stable[91,92] and probably sustain a subsurface biosphere[93–95]. The other type of low-temperature fluid emission is diffuse flow directly within sulfide structures, where high-temperature fluid mixes with seawater as it moves through the porous walls of the mounds. Both types of diffuse flow support complex microbial and macrofaunal communities that are different from those at vent sites with focused flow[10,96]. Diffuse fluid flow is also important in slow-spreading environments and influences the alteration of mantle rocks and serpentinization processes. Peridotite-hosted systems have highly complex and variable vent chemistry, which we discuss in more detail in later sections.

Phase separation

In addition to water–rock reactions, two important processes – boiling and condensation of brines – affect vent fluid compositions in all high-temperature environments[97–100] (Fig. 3c). Because seawater contains 3.2 wt% NaCl, it behaves differently from pure water as it is heated[97]. As seawater migrates to depth, at temperatures above 407 °C and pressures above 298 bar (2,980 m at hydrostatic pressure), the fluids separate into droplets of brine and a lower-salinity vapour phase. This process is called supercritical phase separation or brine condensation. These processes partly govern gas concentrations (for example, CO_2, H_2S and H_2) and are important in partitioning chloride and metals. The development of low-salinity vapours (<3.2 wt% NaCl) and brines (up to 10 wt% NaCl) by phase separation is inferred to be an active process throughout the oceanic crust and is documented in diverse magmatic rocks (Fig. 3c; Supplementary Data). As hydrothermal systems wane and cool, the brines can be entrained into upwelling fluids (for example, Endeavour fluids reach twice normal seawater salinities) or released during eruptive events[101,102]. Brines in the subsurface support distinct, high-temperature, anaerobic microorganisms (halophiles) that tolerate very high NaCl concentrations and metal-rich fluids[103].

Extreme phase separation was documented at the Turtle Pits and Comfortless Cove hydrothermal fields at 5° S MAR, where 407 °C black smoker chimneys were emitting gas bubbles and chloride-depleted fluids (224 mM Cl) with respect to seawater values (545 mM Cl)[104,105]. At 3,000 m depth, venting was occurring at pressure–temperature conditions near the critical point of seawater-salinity fluids. A short burst of fluid (20 seconds) in the Comfortless Cove field was measured at 464 °C, clearly above the critical point and far higher than previously measured fluid temperatures[105] (Fig. 3c). The low-salinity fluids were enriched in Fe, Cu, Co and Mo[106], reflecting the extremely high temperature of the fluids and the importance of phase separation and chloride-complexing in metal transport.

High-temperature fluids and their vapour-dominated nature are influenced by volcanic activity[40,107,108]. For example, following a dyking

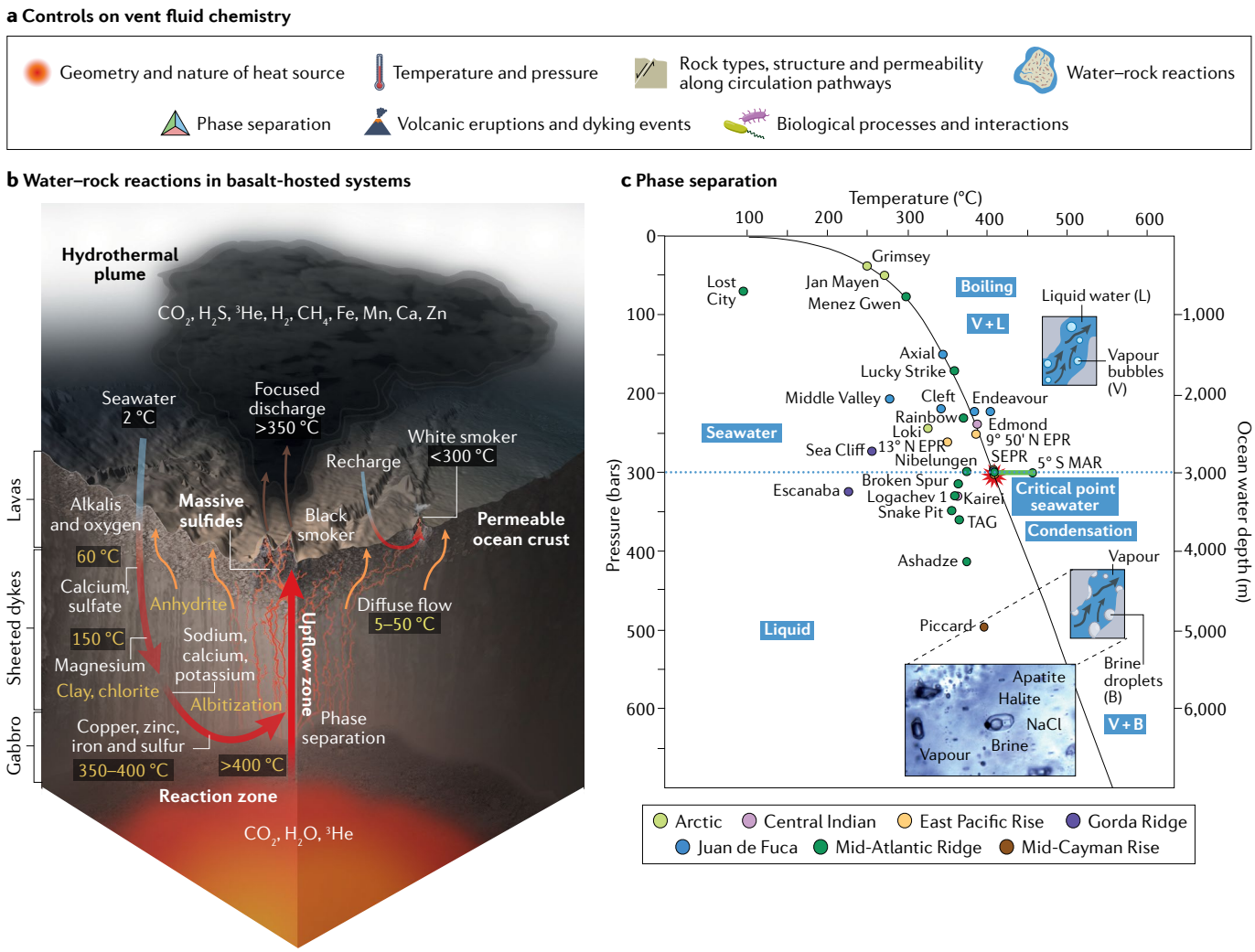

Fig. 3 | Hydrothermal processes at mid-ocean ridges. a, Summary of factors that influence hydrothermal activity and fluid chemistry at MORs. **b**, Conceptual sketch of water–rock reactions and flow paths in an idealized basalt-hosted seafloor hydrothermal system[31,87]. Hot fluids rise buoyantly to the seafloor, where metal-rich, superheated fluids are expelled into the ocean, precipitating metals and forming black and white smoker edifices. **c**, Plot of maximum measured temperatures and pressures of fluids issuing from hydrothermal vents (Supplementary Data). The two-phase boundary (black line) and critical point (407 °C, 298 bar) of seawater[97] are shown with labels indicating the boiling and condensation fields. Inset diagrams show how volatiles partition preferentially into the less dense phase[31,97]. Inset image is of magmatic fluid inclusions (700 °C) in gabbros from the MARK area[98]. EPR, East Pacific Rise; SEPR, southern East Pacific Rise; MAR, Mid-Atlantic Ridge; MARK, Mid-Atlantic Ridge, Kane Fracture Zone; TAG, Trans-Atlantic Geotraverse. Panel **b** produced by the Center for Environmental Visualization, University of Washington.

event at the Main Endeavour Field in 1999, the 380 °C edifice named Puffer at a depth of 2,200 m was venting fluids with one of the lowest chlorinities ever measured (19 mM Cl). In 1998, a temperature of 405 °C was measured at the Brandon Vent on the southern EPR with fluids that varied from below to above seawater salinities[109]. At pressures and depths greater than the critical point of seawater, all vent fluid temperatures fall far off the two-phase curve, many of which occur along the MAR (Fig. 3c; Supplementary Data). Vent temperatures and fluid chemistry suggest that substantial cooling occurs during ascent of the fluids. On the Mid-Cayman Rise, 401 °C fluids from the Piccard site are thought to have phase-separated at temperatures in excess of 500 °C and deeper within the crust[84].

Impact of magmatic events

The large volume of melts at MORs is an important reservoir for volatiles and plays a key role in transferring gases such as CO_2 and He from the mantle to the hydrosphere. Perhaps more than any other factor, volatiles provide a common thread that link geodynamic, geological and geobiological processes in submarine environments. Pronounced changes in seismic activity, permeability, heat flux, temperature and vent fluid chemistry result from intermittent dyking and volcanic eruptive or tectonic events at MORs[40,86,108,110]. Large increases in CO_2 could precede volcanic events, as documented at the Main Endeavour Field following an earthquake swarm in 1999[40,111,112]. Lava interacting with hydrothermal circulation cells produces extreme changes in

water–rock reactions and the nature and degree of phase separation. These events also provide nutrients and energy to microbial populations[113], alter macrofaunal communities and produce large deep-sea hydrothermal plumes in the water column[114].

An important feature of submarine dyking-eruptive events is the formation of 'megaplumes', characterized by the sudden voluminous release of volatiles into the water column, anomalous heat and He relationships, and elevated Mn and Fe that can persist 2–5 years (see review in ref.[42]). The buoyant megaplumes can rise 1,000 metres or more above the surrounding seafloor and can be 20 km across and 70 km in length[114,115]. Estimates of the relative heat flux indicate a sixfold increase during eruptions[36]. Magmatic volatiles released during emplacement of melt into water-saturated porous oceanic crust provide nutrients for massive microbial blooms that accompany eruptions[116–119]. Expulsion of microbial floc and formation of snowblowers was first documented at EPR 9° 50′ N[29] and has been observed at Axial Seamount and on the CoAxial segment of the JdF[35]. This snowblower phenomenon probably occurs during and after most dyking and/or eruptive events and is the result of explosive growth of sulfide-oxidizing bacteria during mixing of large volumes of hydrothermal fluid with oxygenated seawater below the seafloor[120]. These observations and studies of microbes thriving within low- to moderate-temperature diffuse flow fluids have been key in forming the hypothesis that there is a vast, but largely unexplored, diverse microbial biosphere in the crust near to volcanoes and active submarine hydrothermal systems[94,121,122].

Sediment influence

Where ridges are near continental margins, spreading centres can be covered by sediment and are thus classified as sedimented ridges. The presence of a low permeability, insulating blanket of sediment over more permeable volcanic basement directly influences heat and fluid fluxes and the chemistry of the hydrothermal systems that are commonly rich in hydrocarbons[123–125]. The best-studied sedimented MORs are Middle Valley on the JdF[126,127], the Escanaba Trough on the Gorda Ridge[127–129], and the Guaymas and Pescarado Basins in the Gulf of California[124,130,131]. The chemistry of hydrothermal fluids rising through the sediment cover is metal-poor and enriched in CH_4, NH_4 and higher hydrocarbons as a consequence of thermogenic decomposition of organic matter[132] (Table 1; Supplementary Data).

High CH_4 and NH_4 and low values for $\delta^{13}CH_4$ (ref.[133]), as well as elevated B, $\delta^{11}B$, Br, I, Li, Rb and Cs, distinguish Endeavour from many other black smoker systems and led to the concept of a bare-rock, sediment-influenced hydrothermal system[133,134]. The sedimentary component at Endeavour has been hypothesized to be Pleistocene turbidite flows from the Vancouver Island continental margin that are buried at depth[133]. Such turbidite flows buried the Middle Valley hydrothermal site under thick sediments and currently lap to within 200 m of the axial valley at the northern end of the Endeavour Segment. Stable and radiocarbon isotope studies[135] showed that sediments also supply a portion of CO_2 to the vent fluids. Another known sediment-influenced vent system is Loki's Castle on the ultraslow-spreading Arctic Ridge, which is also enriched in barium[136,137].

In summary, oceanic spreading centres are sites of variable but extensive hydrothermal circulation that affects exchange between seawater and the lithosphere and provides nutrients for microbial activity on and below the seafloor. In addition to subsurface lithologies and water–rock–microbe interactions, phase separation and magmatic events are important factors that influence vent fluid compositions. Crustal architecture, magma supply and hydrothermal activity are particularly diverse at the slow-spreading MAR, as discussed in the following sections.

The impact of serpentinization

A number of hydrothermal systems along the slow-spreading MAR are hosted in ultramafic and gabbroic rocks. These include the Rainbow (36° N), Logatchev (14° 45′ N) and Ashadze vent fields (12° 58′ N)[138,139]

Table 1 | Summary of end-member hydrothermal system characteristics

Host rock	Sulfide systems		Sediment-hosted and sediment-influenced systems	Carbonate systems (Lost City type)
	Hosted in basalt or gabbro	Hosted in gabbro and/or serpentinized peridotite	Hosted in basalt, sediment cover, or influenced by sediments at depth	Hosted in serpentinite (±gabbro)
Heat source	Driven by cooling of magma/volcanic crust or gabbroic bodies	Driven by cooling of magma or gabbroic bodies; influenced by serpentinization	Driven by cooling of magma/volcanic crust; interaction with sediments along flow path	Driven by lithospheric cooling and influenced by serpentinization processes
Fluid temperature	High *T*: up to 400 °C	High *T*: 300–360 °C	High *T*: 280–320 °C	Low-moderate *T* <120 °C
pH	Low pH: 2–5	Low pH: 3–4	Moderate pH: 5–6	High pH: 10–11
Element enrichments	Enriched in metals (Fe, Cu, Mn, Zn, Pb) and Si	Enriched in metals (Fe, Cu, Mn, Zn) and variable Si	Variably enriched in metals, enriched in organic C	Low metal concentrations
Volatiles	High CO_2; variable H_2S, CH_4, H_2	High CO_2, CH_4, H_2 and organic compounds; variable H_2S	High CH_4, NH_4^+; variable H_2S, CO_2, H_2	High H_2, CH_4, C2–C4s and organic acids; variable H_2S; negligible CO_2
Type of hydrothermal deposits	Metal-sulfide chimneys and stockworks in basement	Metal-sulfide chimneys and stockworks in basement	Metal-sulfide chimneys and stockworks in basement	Carbonate–brucite chimneys and carbonate in basement
Venting characteristics	Black and white smokers	Black (and white) smokers	Black and white smokers	Not 'white' smokers. Clear 'non-smoking' fluids

Note: Compilation of vent distributions and fluid compositions in Supplementary Data.

Box 2

Serpentinization and volatiles in the oceanic lithosphere

The discovery of hydrothermal vents influenced by serpentinized ultramafic upper mantle rocks — and in particular, the discovery of the off-axis Lost City vent field — has had a key impact on the overall understanding of the role of slow-spreading ridges in global hydrothermal fluxes and the potential impacts of serpentinization[218] (Fig. 4c).

Serpentinization involves hydration of mantle olivine and pyroxene, which produces hydrogen and incorporates up to 14 wt% H_2O. Serpentinization decreases bulk density (to 2.5–2.9 g cm^{-3}) and seismic velocities (V_p < 6 km s^{-1}), and directly affects the strength and physical properties of the mantle, and the magnetic and gravity signatures of the oceanic lithosphere[246,247]. The depth to which serpentinization can occur is controlled by the depth to which seawater can penetrate into the oceanic lithosphere and is largely controlled by tectonic processes and fracture permeabilities. The depth and spatial extent of serpentinized oceanic peridotites has direct consequences for the interpretation of seismic velocity data and can influence where geophysicists estimate the location of the seismic Moho. In addition, the presence of gabbroic intrusions in mantle peridotites leads to Si mobility and talc formation during alteration, which can influence the strength of the lithosphere along detachment faults and aid in uplift and emplacement of mantle sequences at the seafloor.

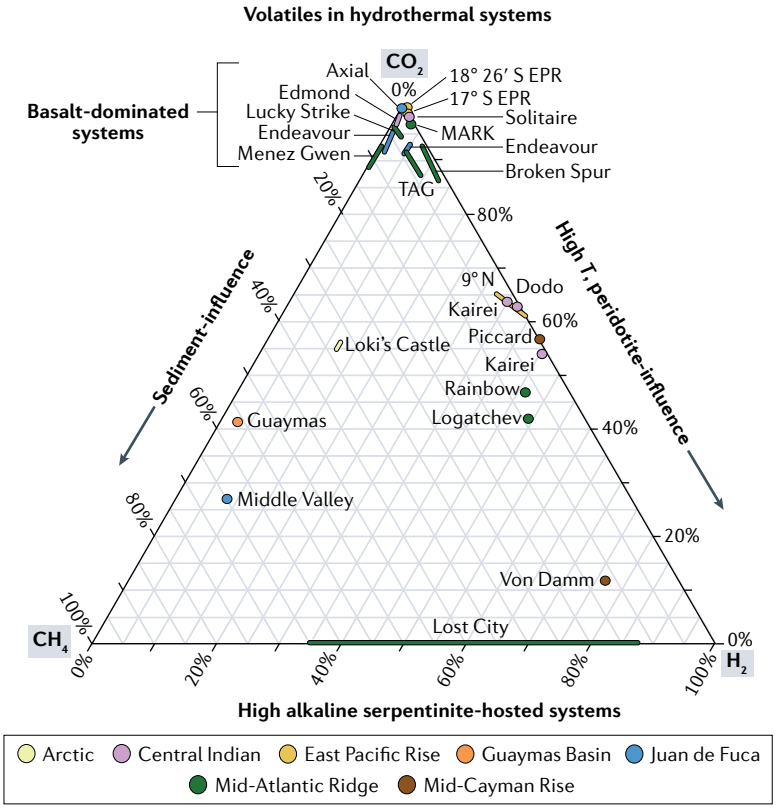

Serpentinization reactions are associated with the uptake or release of many components, such as H_2O, Mg, Ca, Si, Cl, Li, B, C and S (refs.[218,238,248,249]), which can be recycled through subduction and affect subduction-zone dynamics and the compositions of arc magmas[202]. In addition, serpentinization reactions lead to highly reduced fluids with high concentrations of H_2, which distinguishes peridotite-hosted systems from basalt-dominated or sediment-influenced systems (see figure and Supplementary Data; EPR, East Pacific Rise; TAG, Trans-Atlantic Geotraverse; MARK, Mid-Atlantic Ridge, Kane Fracture Zone). Hydrogen production is linked to oxidation of ferrous iron in mantle minerals to produce magnetite during serpentinization, which is limited by brucite formation and incorporation of Fe in other alteration phases in oceanic serpentinites[218,250,251].

Fluids in serpentinizing environments characteristically have elevated concentrations of methane, formate, ethane, propane and other straight-chain hydrocarbons[152,156,177]. H_2 production and the formation of organic molecules and reduced C-species have been considered to occur through abiotic reactions, catalysed by Fe-, Ni- and Cr-bearing minerals, and have important consequences for global chemical cycles and biological activity on and within the seafloor[218]. The geochemical reactions that occur during serpentinization could have been key in early biochemical evolution, which potentially has major implications for the origin and evolution of life on Earth and other planets[145–147].

and the off-axis Lost City hydrothermal field (30° 07′ N)[65,80]. These systems vary in venting temperature, fluid composition and type of hydrothermal deposit, but all characteristically have high CH_4 and H_2, attributed to seawater interaction with gabbroic and ultramafic rocks along the circulation pathways[65,140]. High H_2 concentrations especially mark the influence of serpentinization processes on fluid chemistry[141–144] (Box 2, Supplementary Data). Such systems with highly reducing H_2-rich fluids have gained particular interest because of the potential for abiotic reduction of dissolved inorganic carbon (DIC) to form organic compounds and their potential role in prebiotic chemistry and the origin of life on Earth and perhaps other planets[145–147].

High-temperature peridotite-hosted systems

Key differences between high- and low-temperature peridotite-hosted systems are observed in pH, temperature and CO_2 contents, which, in addition to differences in trace element concentrations and mantle

$\delta^{13}C$ values of CO_2[138,148], point to magmatism as an important source of heat and CO_2 at slow-spreading ridges (Table 1). The Rainbow, Logatchev and Ashadze fields are black smoker systems, in which sulfides are deposited from low-pH (pH ~3.3), high-temperature (350–365 °C), metal-rich fluids with high concentrations of CO_2, CH_4, H_2, and higher hydrocarbons[138,140,149] (see figure in Box 2). Rainbow vent fluids have high chlorinity (above seawater concentrations) indicative of supercritical phase separation (Fig. 3c) and contain the highest dissolved Fe of any MOR vent fluid yet studied[150] (Supplementary Data). Elevated CH_4 and H_2 in MAR high-temperature vents probably reflect a gabbroic and ultramafic influence in the subsurface[140,151,152]. Heat output from Rainbow has been estimated at 1–5 GW (ref.[153]), which is the largest heat flux yet discovered. High heat and fluid output, the formation of sulfide deposits, low pH, and high CO_2 and Fe concentrations in the fluids all suggest that hydrothermal circulation in high-temperature peridotite-hosted systems is likely to be driven by crystallizing magma within the lithospheric mantle. A magmatic heat source is consistent with seismically imaged magmatic sills beneath the Rainbow hydrothermal field[154].

Lost City

The Lost City hydrothermal field on the Atlantis Massif (MAR 30° N) is the first discovered end-member for serpentinite-hosted, hydrothermally active systems devoid of magmatic activity[65,80] and is likely to be an analogue for the Old City vent field on the SWIR[81]. Lost City is the furthest off-axis submarine venting environment and is dominated by variably altered peridotite with gabbroic lenses in the subsurface[66,155]. The fluids are 40–116 °C and alkaline (pH 10–11), with very low CO_2 and metal concentrations, and high CH_4, H_2, formate and higher hydrocarbons[65,156–158] (Box 2; Supplementary Data). Hydrothermal circulation is thought to be driven by residual crustal heat and lithospheric cooling, with fluid compositions primarily controlled by serpentinization reactions[65,159], and fluid discharge controlled by normal faults[66]. Mixing of the alkaline fluids with ambient seawater produces up to 60-m-high, carbonate–brucite towers within the field (Fig. 2f; Supplementary Movies 3 and 4) and results in carbonate deposits along pre-existing, subparallel deformation structures in the detachment fault zone[65,66,159,160].

Because the hydrothermal carbonate structures are bright white (Fig. 2f), the Lost City vents have erroneously been referred to as white smokers. However, white smoker vents are part of evolved, high-temperature, basalt-hosted sulfide systems, located distal to the main upflow zone (Fig. 3b) and emit lighter-hued minerals, rich in barium, calcium, sulfate or silicon, leading to the precipitation of anhydrite at temperatures higher than 150 °C and barite towards lower temperature[88]. In contrast, the Lost City fluids are clear, commonly diffuse, and essentially devoid of mineral or metal particles (Table 1).

H_2 export and DIC uptake

Serpentinization has consequences for H_2 fluxes in hydrothermal systems[47,158,160] (Box 2). Water-column studies and in situ monitoring while drilling across the Atlantis Massif indicate widespread release of H_2 (up to 44 nM) into the water column and elevated H_2/CH_4 ratios that are distinct from channelled flow at Lost City[155,160,161]. In addition, radiocarbon data and distinctly low concentrations of CO_2 in the fluids have been used to argue that modern seawater DIC must be lost within the circulation paths, probably deposited as carbonate in the basement rocks[156,162,163]. A similar uptake of seawater bicarbonate was documented at Endeavour[135] and at 9° 50′ N, suggesting that hydrothermal systems in general could be an important sink of DIC from seawater, stored as carbonate in the rocks[156]. Natural carbon uptake in thermodynamically stable carbonate minerals has now been recognized as a potential mechanism of permanently removing CO_2 from the atmosphere[164] and could help to stabilize atmospheric greenhouse gas concentrations.

Timescales on which such hydrothermal fluids circulate through the oceanic lithosphere remain poorly constrained for most MOR environments, which has limited the understanding of geochemical processes that depend on time. The short-lived radionuclide ^{223}Ra (half-life 11 days) is abundant in Lost City fluids and has been used to constrain subsurface fluid residence times to less than 0.5–2 years[165]. These timescales are surprisingly similar to estimates from seafloor vents in volcanic-hosted systems[166,167] and are probably short enough to allow complex organic molecules to be exported into the overlying water column before they are destroyed. Short residence times also have important implications for understanding hydrothermal carbon transformation reactions that could have led to the formation of the first biomolecules and possibly early life on Earth[168].

CH_4 formation

Processes leading to reduced carbon species in marine hydrothermal systems and the role of serpentinization in CH_4 formation have become controversial[84,169,170]. Methane in peridotite-hosted systems (Box 2) has long been attributed to abiotic Fischer–Tropsch or Sabatier reactions in ultramafic rocks[156,171], where hydration of olivine during serpentinization produces highly reducing conditions and H_2, leading to abiotic reduction of CO_2 to CH_4. Based on studies of fluid inclusions in SWIR gabbros[172,173], field and clumped isotope studies in the past decade suggest that gabbroic intrusions are also a potential source of CH_4 in hydrothermal systems[84,174,175]. Such studies postulate that CH_4 possibly forms in olivine-rich rocks early in the system when temperatures are hotter, is stored as fluid inclusions[84,169], and then is stripped from the rocks into modern fluids during hydrothermal circulation. The origin and the importance of CH_4 for microbial life on Earth and other planets are an active area of research, and the processes of CH_4 production in marine ultramafic settings remain disputed[169,170].

Continued investigations of hydrothermal systems along the MAR and SWIR emphasize the importance of discontinuous magmatism and faulting that result in asymmetric ridge segments, exposure of gabbroic and ultramafic rocks, and marked differences in hydrothermal vent systems at slow-spreading ridges. In contrast to high-temperature systems, Lost City type systems are devoid of magmatic activity and driven by serpentinization processes and faulting.

Microbial diversity at hydrothermal vents

In this section, the marked differences in microbial communities between volcanic-hosted and peridotite-hosted hydrothermal systems[93,122,176] are discussed. Magma-driven systems sustain a high diversity of Bacteria and Archaea due to pronounced physical, thermal and chemical gradients that support a wide range of habitats (Fig. 4). In contrast, low-temperature, serpentinite-influenced systems devoid of magmatic activity, such as Lost City, support a low diversity of microorganisms (and macrofauna) and are dominated by CH_4-metabolizing archaea[177–179].

Diversity at magma-driven vents

Temperature and degree of seawater mixing between seawater and hydrothermal fluids are important determinants of high microbial diversity at magma-driven vents, as these factors affect the availability

a Potential metabolic energy sources and reactions in hydrothermal vent environments

Electron donors	Electron acceptors
H_2, H_2S, CH_4, NH_3, S^0, $S_2O_3^{2-}$, Mn^{2+}, NO_2^-	+ O_2
H_2, H_2S, S^0, $S_2O_3^{2-}$, Fe^{2+}	+ NO_3^-
H_2S, S^0	+ NO_2^-
H_2	+ MnO_2
H_2	+ Fe^{3+}
H_2	+ S^0
H_2, CH_4	+ SO_4^{3-}
H_2	+ CO_2

Oxidizing

Increasing T

General trend of decreasing energy yield

Reducing

Aerobic reactions

1. Metal (iron II) oxidation
   $4Fe^{2+} + O_2 + 10H_2O \rightarrow 4Fe(OH)_3 + 8H^+$
2. Sulfide oxidation
   $H_2S + 2O_2 \rightarrow SO_4^{2-} + 2H^+$
   $5HS^- + 8NO_3^- + 3H^+ \rightarrow 5SO_4^{2-} + 4N_2 + 4H_2O$
3. Methane oxidation
   $CH_4 + 2O_2 \rightarrow CO_2 + 2H_2O$
   $CH_4 + 2O_2 \rightarrow HCO_3^- + H^+ + H_2O$
4. Hydrogen oxidation
   $2H_2 + 2O_2 \rightarrow 2H_2O$
   $5H_2 + 2NO_3^- \rightarrow N_2 + 4H_2O + 2OH^-$

Anaerobic reactions

5. Anaerobic iron oxidation
   $8Fe^{2+} + 10H^+ + NO_3^- \rightarrow 8Fe^{3+} + NH_4^+ + 3H_2O$
   $10Fe^{2+} + NO_3^- + 12H^+ \rightarrow 10Fe^{3+} + N_2 + 6H_2O$
6. Nitrate reduction
   $H_2 + NO_3^- \rightarrow NO_2^- + H_2O$
7. Sulfate reduction
   $4H_2 + 2H^+ + SO_4^{2-} \rightarrow H_2S + 4H_2O$
8. Methanogenesis with $\sum CO_2$
   $4H_2 + CO_2 \rightarrow CH_4 + 2H_2O$
9. Methanogenesis with formate
   $4HCCO^- + H_3O^+ \rightarrow 3HCO_3^- + CH_4$
10. Anaerobic methane oxidation
    $CH_4 + 2H^+ + SO_4^{2-} \rightarrow H_2S + CO_2 + 2H_2O$

b Black smoker flow paths, fluid–rock interaction and ecosystems

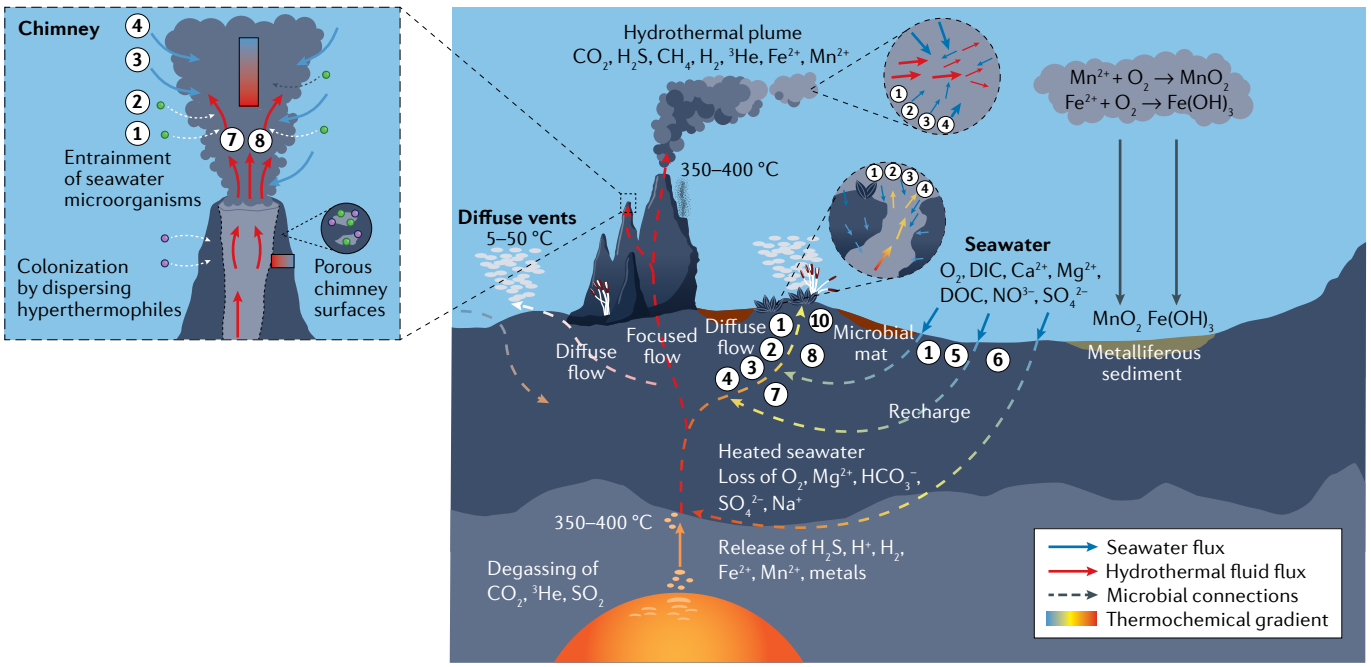

c Lost City type hydrothermal systems

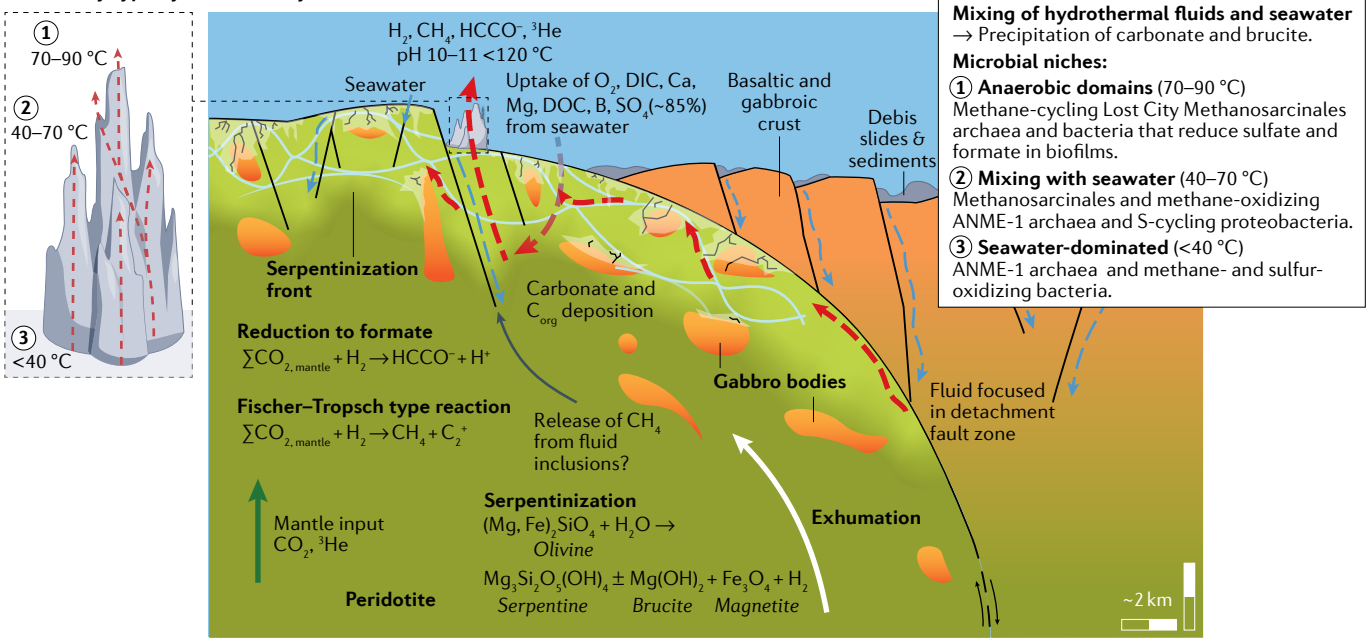

Mixing of hydrothermal fluids and seawater → Precipitation of carbonate and brucite.

Microbial niches:

1. **Anaerobic domains** (70–90 °C) Methane-cycling Lost City Methanosarcinales archaea and bacteria that reduce sulfate and formate in biofilms.
2. **Mixing with seawater** (40–70 °C) Methanosarcinales and methane-oxidizing ANME-1 archaea and S-cycling proteobacteria.
3. **Seawater-dominated** (<40 °C) ANME-1 archaea and methane- and sulfur-oxidizing bacteria.

Fig. 4 | Mid-ocean ridge hydrothermal fluxes and life. a, Variations in availability of electron donors and electron acceptors under varying temperature and redox conditions, and their potential metabolic energy sources. Examples of general inorganic redox reactions along thermochemical mixing gradients in vent environments that support diverse microbial communities, with potential locations along subsurface flow paths in basalt-hosted systems shown as circled numbers on panel **b**. **b**, Representation of fluid flow paths and fluid–rock interactions that govern chemical fluxes, redox reactions and microbial ecosystems at magmatically robust black smoker systems with circulation limited to the upper crust (<2–3 km crustal depth) above axial magma lenses. Reactions 1–4 take place in the shallow subsurface and zones of mixing with seawater and are not restricted to any particular distance from the ridge axis. **c**, Same as **b**, but for a Lost City type system controlled by faults and serpentinization processes[236] (Box 2). Light blue anastomosing network depicts early interconnected fluid pathways leading to the onset of serpentinization[162,237]. Reactions between gabbro lenses and peridotite cause localized silica metasomatism (lightest green patches around gabbroic bodies in serpentinized domains)[155,238]. ANME-1, anaerobic CH_4-oxidizing archaea; DIC, dissolved inorganic carbon; DOC, dissolved organic carbon. Panel **b** is adapted from ref.[239], CC BY 2.0 (https://creativecommons.org/licenses/by/2.0/). Inset in **b** adapted from ref.[96], Springer Nature. Panel **c** adapted with permission from ref.[162], Wiley.

of electron acceptors and donors, and thus the energy-yielding microbial metabolisms[96] (Fig. 4). Different groups of vent-associated Bacteria and Archaea have been shown to grow over the temperature range of 2 °C, in surrounding seawater and hydrothermal vent plumes[96], to at least 122 °C in hot subsurface fluids[11,12,93].

Energy sources and redox reactions. In general, above 40–60 °C, oxygen is limiting such that the majority of microorganisms are anaerobic, using elemental sulfur, sulfate, nitrate and CO_2 as electron acceptors (Fig. 4a). CO_2 is the predominant source of carbon for all thermal groups of vent Bacteria and Archaea, although heterotrophs have also been detected, even among some of the thermophilic archaea. In addition to sulfur, high levels of H_2 serve as the energy source for phylogenetically and physiologically diverse groups of Bacteria and Archaea. H_2-utilizing microorganisms have been identified in subsurface, black smoker and vent plume environments, and as animal symbionts[180]. H_2-utilizing proteobacteria dominate the cooler environments, whereas archaeal methanogens dominate the most extreme of the high-temperature environments. The latter are limited in the availability of reduced or oxidized nitrogen sources, but hyperthermophilic methanogens have been isolated that fix N_2 (ref.[181]). Abiotic reactions that can reduce N_2 have also been identified under both volcanic-hosted and peridotite-hosted hydrothermal conditions[182,183]. Whether these reactions provide a source of reduced N for vent microorganisms is unknown.

Porous vent environments influenced by mixing with seawater — varying from subsurface habitats to black smoker chimney structures, and hydrothermal vent plumes advecting through the water column — support a markedly high diversity of bacteria, including aerobes that use seawater-derived electron acceptors such as oxygen, sulfur, CO_2, nitrate, nitrite and nitrous oxide, and various metals including iron[42,96,184,185] (Fig. 4). Many members of vent bacteria derive energy from redox reactions involving electron acceptors such as nitrate and iron coupled to the oxidation of reduced sulfur compounds and H_2 (refs.[184,186,187]). The dominant Archaea isolated from magma-driven vent environments include species from both the Euryarchaeota and the Crenarchaeota. Methanogens are dominant among Euryarchaeota, although Euryarchaeota also include many of the commonly isolated heterotrophic hyperthermophilic (75 °C to >100 °C) archaea, some of which were among the first hyperthermophilic species isolated from hydrothermal vent environments in the 1980s.

Hydrothermal plumes and diffuse fluids. High-temperature hydrothermal vents produce buoyant plumes that harbour a wide range of chemosynthetic microorganisms capable of oxidizing S, H_2, CH_4, Fe and Mn as energy sources and using CO_2 as the carbon source (Fig. 4b). The source of plume microorganisms is the deep ocean, where they are ubiquitous. Active plume microbial communities form a substantial fraction of the deep ocean carbon pool, estimated to be comparable to the particulate organic carbon flux exported from pelagic sources[188].

Studies of low-temperature diffuse fluids at different vents within the same hydrothermal field indicate that individual diffuse flow sites can maintain unique microbial populations over time and have spatially distinct taxonomic, metabolic potential and genetic characteristics[91,92,94]. The ability of an individual site to maintain an active subseafloor population is intrinsically linked to the geochemistry of the system, the mixing conditions, and the geological characteristics of the individual vent site[92,176].

Microbial ecology has been revolutionized by new bioinformatics methods that use genome sequences to identify uncultivated microorganisms and viruses, which provide insight into their physiology and evolutionary history and help to advance culturing techniques. Bioinformatic approaches have resulted in discoveries that not only have identified very high diversity of microorganisms in hydrothermal vent and subseafloor environments and the role of viruses in shaping that diversity, but also have profoundly changed the understanding of the evolutionary history of the microbial world[189]. A key discovery was the identification of the Lokiarchaeota in deep-sea sediments in the Arctic that had episodic hydrothermal input, possibly from the nearby basalt-hosted hydrothermal vents at Loki's Castle[190]. Lokiarchaeota share many characteristics previously thought to be found only in Eukaryotes, thus promising a better understanding of the evolution of the Eukaryotes[14,190,191] and supporting evidence for placing the Eukaryotes as emerging from the archaeal branch of the tree of life[192,193].

Growth rates of hydrothermal vent microorganisms. Most information on growth rates of vent microorganisms comes from laboratory studies of pure cultures. Growth rates can vary with doubling times from minutes to hours. One of the main gaps in understanding the microbial ecology of vent environments is determining in situ growth rates and productivity of microbial communities. This is a difficult task, particularly in diffuse fluids, because of mixing of different physiological groups of microorganisms from different depths that have marked gradients in temperature, electron acceptors and energy sources. An attempt to circumvent these obstacles involved the incubation of vent water samples from the EPR 9° 50′ N at in situ temperature and pressure with and without supplements of electron acceptors[194]. Microbial growth and carbon fixation rates were measured using subsurface water incubated at in situ temperatures of 24 °C and 50 °C with and without O_2, NO_3^- and H_2. The results showed a production rate as high as those found in animal symbiosis and with doubling times of 17–41 hours. The authors identified three genera of the Campylobacteria group that included S and H_2 oxidizers as the dominant microbes. Campylobacteria are common in vent environments and represent 85% of the biomass in sulfide chimneys. Campylobacteria have also been identified as the dominant group in diffuse flow vents and in the shallow subseafloor[96]. Although this study was limited to just one group of the diverse population in vent fluids, it emphasizes that something must limit the accumulation of microbial biomass, given the rapid growth rates.

One possible limit to growth could be the widespread diversity of viruses including both free-living and lysogenic (associated with the host genome) that are present in specific vent environments[195]. The rate of virus lysis of vent microbes or the rate and specific genes transferred by virus to bacteria is unknown. Moreover, there is evidence of protist grazing of vent bacteria that appears to be particularly substantial in diffuse flow vent environments and, based on bacterial productivity rates[194], protists grazing could account for up to 22% of chemosynthetic populations[196].

Diversity at serpentinite-hosted vents

The microbial ecology of marine serpentinite-dominated vent environments is known largely from Lost City. Less information is available from the more recently discovered site Old City vent field at the SWIR[81] or from Logatchev and Rainbow. Early microbiology studies at Lost City showed a very low diversity of microorganisms, with CH_4-metabolizing archaea dominating at active, moderate-temperature, anaerobic carbonate chimneys, and sulfur-metabolizing proteobacteria occupying the lower-temperature, oxic or anoxic chimney environments[65,179,197] (Fig. 4c). The CH_4-metabolizing archaea, which are related to the Methanosarcinales, exist as complex biofilms within young, active carbonate chimneys. As the chimneys age and hydrothermal input decreases, the dominance by Methanosarcinales shifts to complete dominance by anaerobic CH_4-oxidizing archaea (ANME-1)[198]. Rare microbial taxa in the youngest samples are progressively more dominant in older samples, suggesting that the Lost City microbial community and perhaps other similar serpentinization environments are preadapted to reoccurring environmental changes as an example of long-term ocean memory[199].

Molecular (DNA-based) characterization of the Lost City Methanosarcinales biofilm has shown their potential to fix N_2 and, based on an extraordinary abundance of transposable elements, a potential for a very high incidence of gene transfer[200,201]. In laboratory experiments, this biofilm has both produced and anaerobically oxidized CH_4, enhanced by H_2 (ref.[201]). Low concentrations of CO_2 in Lost City fluids indicates that these Methanosarcinales might use alternative sources of carbon for CH_4 production, such as formate or acetate[157] (Fig. 4c). The observation that sulfate-reducing bacteria convert formate to CO_2 (ref.[177]) has led to the hypothesis that this CO_2 is then converted to CH_4 (ref.[178]). The Lost City Methanosarcinales biofilm shows multiple morphologies, including cells with stacked, intracellular membranes similar to morphologies of aerobic methane-oxidizing bacteria, and might thus have some cells that oxidize methane anaerobically[201]. Many questions remain about the Lost City microbial community, particularly regarding Methanosarcinales, including their in situ growth and activity rates, their diversity in physiologies and potential syntrophic interactions.

Summarizing, magma-driven hydrothermal systems host a vast, hot and diverse microbial biosphere that sustains thriving macrofaunal communities at vents and contributes a substantial fraction of the deep ocean carbon pool. In contrast, high-pH serpentinizing hydrothermal systems harbour distinctly more limited microbial communities dominated by methane-metabolizing archaea.

Global fluxes and biogeochemical cycles

Hydrothermal circulation at MORs and ridge flanks controls global heat fluxes and plays an important role in regulating seawater chemistry, biogeochemical cycles, and input fluxes into subduction zones[87,202]. Although rates and directions of chemical exchange vary, hydrothermal processes are an important sink for seawater Mg, sulfate and P, and a source of volatiles and many elements, such as Fe and Mn and other metals[203], that serve as energy sources for microbial ecosystems at and beneath the seafloor.

Heat flux

Most estimates of hydrothermal chemical fluxes combine convective heat output with compositional differences between hydrothermal fluids and seawater. A problem with this approach is to properly apportion heat flow between on-axis and ridge-flank regions. Current estimates put this distribution at 1.8 ± 0.3 TW and 8.1 ± 2 TW (ref.[7]), respectively. Other estimates of heat flux use magma input, which lead to an average value of 50 MW km^{-1} (~3 TW) for the entire ridge system[204], or combine hydrothermal fluid concentrations with the compositions of the rocks in the subsurface[205], both of which tend to be lower than those using heat flux. However, vent fluid compositions can change greatly with time, particularly following magmatic and seismic events[108,110], and we do not yet have an adequate understanding of the role played by these events relative to the steady-state flux.

Magnesium and calcium

The long-standing Mg problem, which recognized that the riverine input of Mg was much larger than the known sinks[206], was notably improved by the discovery of Mg uptake in hydrothermal systems[207]. It is estimated that high-temperature vent systems take up ~37% of the riverine Mg input and that low-temperature alteration on ridge flanks accounts for another ~14%[6]. Modern dolomite formation might account for a major fraction of the remaining Mg sink, as indicated by Mg isotopes[208]. Although hydrothermal processes are both a sink and source of Ca, the net flux of Ca is to the oceans[203] and is ~20% of riverine input[6]. An extensive list of elements and compounds can be found elsewhere[203].

Organic carbon

Hydrothermal systems contribute to global carbon budgets by providing a notable fraction of organic carbon to the deep ocean through microbial activity and oxidation of organic compounds[188]. Heterotrophic microbial production rates are estimated to be up to 0.9 gC m^{-2} yr^{-1} and could contribute 0.05 GtC yr^{-1} of the particulate organic carbon (POC) within hydrothermal plumes, similar to POC export fluxes of ~3 gC m^{-2} yr^{-1} estimated for the deep Atlantic and Pacific oceans[188]. Hydrothermal processes also influence the composition and fluxes of dissolved organic carbon (DOC) to the ocean[209]. A large fraction of the deep ocean DOC is refractory[210] and ranges from 4,000 years old in the North Atlantic to 6,000 years in the North Pacific[211]. High-temperature hydrothermal circulation alters and largely destroys DOC; however, diffuse vent fluids contain higher DOC than deep seawater, which has been attributed to subsurface microbial communities[212,213]. Ridge-flank fluids contain less DOC than deep seawater and can be as old as 17,000 years[212,214,215]. DOC older than deep North Atlantic water was also found emanating from cold oceanic crust at North Pond near the MAR[216]. These data coupled with findings of 6,900-year-old DOC near the East Pacific Rise at 25° S[217] have led to the speculation that hydrothermal venting could be an important source of old DOC to the deep ocean[209].

Hydrothermal circulation can also lead to the incorporation of DOC in basement rocks; total organic carbon could be up to ~1,500 ppm in oceanic ultramafic and up to ~600 ppm in gabbroic rocks[218,219]. Stable isotope and radiocarbon studies of the Atlantis Massif[163] indicate that organic carbon with an average radiocarbon age of 14,000 years is incorporated during serpentinization and suggest that

Glossary

Abiotic
Formed or characterized by the absence of life or living organisms.

Aerobic
Pertaining to or requiring the presence of free oxygen.

Anaerobic
Occurring, living or active in the absence of free oxygen.

Asthenosphere
The viscous, mechanically weak and ductile region of the upper mantle between approximately 80 and 200 km depth that is involved in plate tectonic dynamics.

Chemosynthesis
The synthesis of organic compounds by microorganisms using energy derived from inorganic chemical reactions.

Critical point of seawater
Pressure and temperature conditions at which solid, liquid and vapour phases of seawater coexist in thermodynamic equilibrium.

Gabbro
Igneous rock (formed from crystallization of magma) consisting primarily of varying proportions of the minerals plagioclase and pyroxene.

Heterotrophs
Organisms that are incapable of making their own food from light or inorganic compounds but consume complex organic compounds or other organisms in a food chain.

Hydrothermal plumes
Upwelling and dispersal of buoyant hydrothermal fluids into the ocean at hydrothermal vents or after eruptions or dyking events.

Hyperthermophilic
Pertaining to microorganisms that thrive in extremely hot environments and optimally grow above 80 °C.

Lithosphere
Outer solid layer of the Earth, consisting of the brittle crust and uppermost mantle.

Magma lenses
During periods of enhanced magma replenishment at MORs, magma accumulates in an axial melt lens overlying smaller stacked sills beneath sheeted dykes.

Microbial floc
Microbial aggregates that appear as cloudy suspensions of cells floating in seawater rather than attached to a surface like most biofilms.

Moho
The Mohorovičić discontinuity, known as the seismic Moho, is a discrete change in seismic wave velocities used to define the boundary between the crust and the mantle.

Oceanic detachment faults
Extensional normal faults associated with asymmetric spreading that results in exposure of lower-crustal and upper-mantle rocks on the seafloor.

Oceanic crust
The outermost layer of the lithosphere formed at mid-ocean ridge (MOR) spreading centres; it is 5–10 km thick, primarily composed of mafic lavas, dykes and gabbros.

Oceanic crustal architecture
Rock types (lithologies), their distribution and structure of the oceanic crust.

Ophiolite
Segments of oceanic crust and upper mantle tectonically exposed on land, often preserving features observed in different tectonic settings on the seafloor.

Peridotite
The dominant rock type in the Earth's upper mantle, consisting primarily of the Mg-rich minerals olivine and pyroxene.

pH
A logarithmic scale from 0 to 14 to indicate the concentration of hydrogen ions in an aqueous solution and specifies the acidity (pH < 7) or basicity (pH > 7) of the solution.

Serpentinization
Hydrothermal process that transforms anhydrous Fe–Mg silicates into hydrous minerals, such as serpentine and brucite, producing magnetite and hydrogen.

Snowblowers
A distinct form of low-temperature hydrothermal venting with expulsion of copious amounts of white flocculent microbial material, reminiscent of snow.

Spreading rate
The rate at which new oceanic lithosphere is created at mid-ocean ridge plate boundaries resulting in seafloor spreading.

Volatiles
Dissolved gases in hydrothermal fluids or exsolved from melts.

oxidation of organic compounds along circulation paths could provide carbon for carbonates. Annual storage rates of up to 1.7×10^{11} mol C yr^{-1} of organic carbon and up to 6×10^{12} mol C yr^{-1} of inorganic carbon in serpentinized oceanic peridotites have been estimated[163].

Iron

Hydrothermal Fe fluxes to the deep ocean and the impact they could have on primary productivity and nitrogen fixation are currently an exciting area of research. Early studies had assumed that Fe from high-temperature systems would quickly precipitate out of the plumes as sulfide or oxygenated particles. However, Fe can be transported thousands of kilometres across ocean basins away from the hydrothermal source either as nanoparticles or as organically chelated dissolved iron[220]. Current estimates of dissolved Fe flux are $4–6 \times 10^9$ mol yr^{-1} (refs.[220,221]). This flux is thought to be a notable source to the deep ocean that could eventually upwell and promote primary production in the 'high-nitrate low-chlorophyll' (HTLC) regions where Fe is considered to be the limiting nutrient. The Southern Ocean is one of these important HTLC regions, where Fe is thought to lead to phytoplankton blooms[222,223]. Modelling has shown that upwelling of hydrothermal Fe might be responsible for 15–30% of the primary production in this region, thus linking the global biogeochemical cycles of iron and carbon. Iron from shallow hydrothermal plumes at the Tonga–Kermadec Arc is an important component of increased nitrogen fixation and primary production in that region[224,225].

There is currently extensive research on the topic of Fe fluxes, and much to be learned regarding the importance of hydrothermal sources of Fe and other trace metals to the deep ocean. So far, most hydrothermal chemical flux estimates are based on basalt-hosted MOR systems. However, it is well accepted that hydrothermal circulation at all ridges and ridge flanks contributes to global heat fluxes and has an important role in regulating seawater chemistry, the composition of the oceanic crust and biogeochemical cycles. Release of many hydrothermally related compounds to the water column has an immediate effect on chemoorganotrophic activity within hydrothermal plumes, representing a substantial organic carbon export flux in the deep ocean[188]. A full understanding of hydrothermal fluxes requires further research of back-arc spreading centres, island-arc and peridotite-hosted sites as

well as tackling the difficult job of quantifying temporal variability in vent fluids[40,108].

Summary and future perspectives

The theories of plate tectonics and seafloor spreading revolutionized Earth and ocean sciences and paved the way for new oceanographic, analytical and theoretical approaches to understand how the Earth works. However, fundamental gaps remain in understanding the interplay among geological and biogeochemical processes and in quantifying the hydrogeology of hydrothermal systems and the impact of fluid pathways at ridges and ridge flanks on heat, chemical and biological fluxes to the ocean.

The discovery of submarine hydrothermal vents supporting chemosynthetic communities led to revolutionary understanding of the tree of life[190] and the conditions under which life can thrive, survive and die. Indeed, we are beginning to acquire a glimpse of the rare deep biosphere within the lithosphere and hydrothermal vents[95] and have started to make progress towards understanding the importance of viruses[195] and fungi[226] in these systems. However, little is known about how organisms and viruses evolve over time, how these communities interact and to what extent vents are sources for organisms in the overlying ocean.

Advanced sampling, spectroscopic and chromatographic techniques have also started to unravel the compositions, sources and decomposition of DOC and complex organic compounds in hydrothermal systems[227–230]. The continued development of compound specific radiocarbon analyses and new sampling and analytical techniques are needed to further understand the composition, age and fate of seawater and hydrothermally-derived DOC and its potential contribution to deep-ocean DOC.

Technical innovation and installation of ocean observatories have advanced the ability for monitoring and allows for rapid response to magmatic and tectonic activity, providing real-time information on the development of dyking-eruptive events from their inception (Box 1). Advancing these capabilities is vital for future research and will require more sophisticated sensors, cabled and uncabled instrument networks and advanced underwater vehicles[231,232]. Future research will be guided by advances in robotic technologies together with miniaturization and automation of sensor systems[233]. Development of in situ chemical, physical and metagenomic sensors for long-term deployments on the seafloor and in the overlying water column will allow the detection of ephemeral processes that have been missed by traditional oceanographic methods and will provide information on how these systems evolve over time.

Understanding the processes that control the dynamic interplay of geology, chemistry and biology within the oceans and rocks beneath it will become increasingly important as humans continue to influence the Earth's oceans and atmosphere. Continued exploration of hydrothermal environments promises to offer new insights across multiple disciplines. It is vital that these systems are not exploited in ways that could destroy or irreversibly alter them, which would result in lost opportunities for discoveries and limit future insight into the processes that shape the planet. The deep sea holds spectacular wonders, with many more to discover — and much to protect.

Data availability

The compilation of vent distributions and fluid compositions is provided in the online Supplementary Data file.

Published online: 15 November 2022

References

1. Parsons, B. The rates of plate creation and consumption. *Geophys. J. Int.* **67**, 437–448 (1981).
2. Sinha, M. C. & Evans, R. L. Geophysical constraints upon the thermal regime of the ocean crust. *Geophys. Monogr. Ser.* https://doi.org/10.1029/148GM02 (2004).
3. German, C. R. & Lin, J. The thermal structure of the oceanic crust, ridge-spreading and hydrothermal circulation: How well do we understand their inter-connections? *Geophys. Monogr. Ser.* https://doi.org/10.1029/148GM01 (2004).
4. Wheat, C. G., Fisher, A. T., McManus, J., Hulme, S. M. & Orcutt, B. N. Cool seafloor hydrothermal springs reveal global geochemical fluxes. *Earth Planet. Sci. Lett.* **476**, 179–188 (2017).
5. Stein, C. A. & Stein, S. Constraints on hydrothermal heat flux through the oceanic lithosphere from global heat flow. *J. Geophys. Res.* **99**, 3081–3095 (1994).
6. Mottl, M. in *Energy and Mass Transfer in Marine Hydrothermal Systems* (eds Halbach, P. E. et al.) 271–286 (Dahlem Univ. Press, 2003).
7. Wheat, C. G. & Mottl, M. J. in *Hydrogeology of the Oceanic Lithosphere*, 627–658 (Cambridge Univ. Press, 2004).
8. Cavanaugh, C. M., Gardiner, S. L., Jones, M. L., Jannasch, H. W. & Waterbury, J. B. Prokaryotic cells in the hydrothermal vent tube worm *Riftia pachyptila* Jones: possible chemoautotrophic symbionts. *Science* **213**, 340–342 (1981).
9. Lilley, M. D., Baross, J. A. & Gordon, L. I. in *Hydrothermal Processes at Seafloor Spreading Centers* (eds Rona, P. A. et al.) 411–449 (Springer, 1983).
10. Corliss, J. B. et al. Submarine thermal springs on the Galápagos Rift. *Science* **203**, 1073–1083 (1979).
11. Takai, K. et al. Cell proliferation at 122 °C and isotopically heavy CH_4 production by a hyperthermophilic methanogen under high-pressure cultivation. *Proc. Natl Acad. Sci. USA* **105**, 10949–10954 (2008).
12. Kashefi, K. & Lovley, D. R. Extending the upper temperature limit for life. *Science* **301**, 934–934 (2003).
13. Weiss, M. C. et al. The physiology and habitat of the last universal common ancestor. *Nat. Microbiol.* **1**, 16116 (2016).
14. Spang, A. & Ettema, T. J. G. Microbial diversity: the tree of life comes of age. *Nat. Microbiol.* **1**, 16056 (2016).
15. Spiess, F. N. et al. East Pacific Rise: hot springs and geophysical experiments. *Science* **207**, 1421–1433 (1980).
16. Von Damm, K. L. et al. Chemistry of submarine hydrothermal solutions at 21°N, East Pacific Rise. *Geochim. Cosmochim. Acta* **49**, 2197–2220 (1985).
17. Felbeck, H. Chemoautotrophic potential of the hydrothermal vent tube worm, *Riftia pachyptila* Jones (Vestimentifera). *Science* **213**, 336–338 (1981).
18. Beaulieu, S. E., Baker, E. T., German, C. R. & Maffei, A. An authoritative global database for active submarine hydrothermal vent fields. *Geochem. Geophys. Geosyst.* **14**, 4892–4905 (2013).
19. Jannasch, H. W. & Wirsen, C. O. Chemosynthetic primary production at East Pacific sea floor spreading centers. *BioScience* **29**, 592–598 (1979).
20. Hey, R. et al. Tectonic/volcanic segmentation and controls on hydrothermal venting along Earth's fastest seafloor spreading system, EPR 27°–32°S: segmentation along the EPR. *Geochem. Geophys. Geosyst.* https://doi.org/10.1029/2004GC000764 (2004).
21. Carbotte, S. & Macdonald, K. East Pacific rise 8°–10° 30′ N: evolution of ridge segments and discontinuities from SeaMARC II and three-dimensional magnetic studies. *J. Geophys. Res.* **97**, 6959 (1992).
22. Anonymous. Penrose field conference on ophiolites. *Geotimes* **17**, 24–25 (1972).
23. Carbotte, S. M. et al. Stacked magma lenses beneath mid-ocean ridges: insights from new seismic observations and synthesis with prior geophysical and geologic findings. *J. Geophys. Res. Solid Earth* https://doi.org/10.1029/2020JB021434 (2021).
24. Sinton, J. M. & Detrick, R. S. Mid-ocean ridge magma chambers. *J. Geophys. Res.* **97**, 197–216 (1992).
25. Coogan, L. A. The lower oceanic crust. in *Treatise on Geochemistry* 497–541 (Elsevier, 2014).
26. Brown, T. C. et al. Textural character of gabbroic rocks from pito deep: a record of magmatic processes and the genesis of the upper plutonic crust at fast-spreading mid-ocean ridges. *J. Petrol.* **60**, 997–1026 (2019).
27. Maher, S. M., Gee, J. S., Cheadle, M. J. & John, B. E. Three-dimensional magnetic stripes require slow cooling in fast-spread lower ocean crust. *Nature* **597**, 511–515 (2021).
28. Karson, J. A., Kelley, D. S., Fornari, D. J., Perfit, M. R. & Shank, T. M. *Discovering the Deep: a Photographic Atlas of the Seafloor and Ocean Crust*. (Cambridge Univ. Press, 2015).
29. Haymon, R. M. et al. Volcanic eruption of the mid-ocean ridge along the East Pacific Rise crest at 9°45–52′ N: direct submersible observations of seafloor phenomena associated with an eruption event in April, 1991. *Earth Planet. Sci. Lett.* **119**, 85–101 (1993).
30. Von Damm, K. L. et al. Evolution of East Pacific Rise hydrothermal vent fluids following a volcanic eruption. *Nature* **375**, 47–50 (1995).
31. Von Damm, K. L. Controls on the chemistry and temporal variability of seafloor hydrothermal fluids. *Geophys. Monogr. Ser.* (eds Humphris, S. E., et al.) 222–247 (American Geophysical Union, 1995).
32. Tolstoy, M. et al. A sea-floor spreading event captured by seismometers. *Science* **314**, 1920–1922 (2006).
33. Tan, Y. J., Tolstoy, M., Waldhauser, F. & Wilcock, W. S. D. Dynamics of a seafloor-spreading episode at the East Pacific Rise. *Nature* **540**, 261–265 (2016).

34. Tolstoy, M., Waldhauser, F., Bohnenstiehl, D. R., Weekly, R. T. & Kim, W.-Y. Seismic identification of along-axis hydrothermal flow on the East Pacific Rise. *Nature* **451**, 181–184 (2008).
35. Delaney, J. R. et al. The quantum event of oceanic crustal accretion: impacts of diking at mid-ocean ridges. *Science* **281**, 222–230 (1998).
36. Baker, E. T. et al. Posteruption enhancement of hydrothermal activity: a 33-year, multieruption time series at Axial Seamount (Juan de Fuca Ridge). *Geochem. Geophys. Geosyst.* **20**, 814–828 (2019).
37. Clague, D. A. et al. Geologic history of the summit of Axial Seamount, Juan de Fuca Ridge: geologic history of Axial Seamount. *Geochem. Geophys. Geosyst.* **14**, 4403–4443 (2013).
38. Chadwick, W. W., Nooner, S. L., Butterfield, D. A. & Lilley, M. D. Seafloor deformation and forecasts of the April 2011 eruption at Axial Seamount. *Nat. Geosci.* **5**, 474–477 (2012).
39. Wilcock, W. S. D. Physical response of mid-ocean ridge hydrothermal systems to local earthquakes. *Geochem. Geophys. Geosyst.* https://doi.org/10.1029/2004GC000701 (2004).
40. Lilley, M. D., Butterfield, D. A., Lupton, J. E. & Olson, E. J. Magmatic events can produce rapid changes in hydrothermal vent chemistry. *Nature* **422**, 878–881 (2003).
41. Delaney, J. R., Robigou, V., McDuff, R. E. & Tivey, M. K. Geology of a vigorous hydrothermal system on the Endeavour Segment, Juan de Fuca Ridge. *J. Geophys. Res.* **97**, 19663–19682 (1992).
42. Kelley, D. S., Baross, J. A. & Delaney, J. R. Volcanoes, fluids, and life at mid-ocean ridge spreading centers. *Annu. Rev. Earth Planet. Sci.* **30**, 385–491 (2002).
43. Kelley, D. et al. Endeavour Segment of the Juan de Fuca Ridge: one of the most remarkable places on Earth. *Earth Oceanog.* **25**, 44–61 (2012).
44. Clague, D. A. et al. Hydrothermal chimney distribution on the Endeavour Segment, Juan de Fuca Ridge. *Geochem. Geophys. Geosyst.* **21**, e2020GC008917 (2020).
45. Robigou, V., Delaney, J. R. & Stakes, D. S. Large massive sulfide deposits in a newly discovered active hydrothermal system, the High-Rise field, Endeavour Segment, Juan de Fuca Ridge. *Geophys. Res. Lett.* **20**, 1887–1890 (1993).
46. Bird, P. An updated digital model of plate boundaries. *Geochem. Geophys. Geosyst.* **4**, 1027 (2003).
47. Cannat, M., Fontaine, F. & Escartín, J. Serpentinization and associated hydrogen and methane fluxes at slow spreading ridges. in *Geophys. Monogr. Ser.* **188**, 241–264 (2010).
48. John, B. E. & Cheadle, M. J. Deformation and alteration associated with oceanic and continental detachment fault systems: are they similar? *Geophys. Monogr. Ser.* **188**, 175–205 (2010).
49. Escartín, J. et al. Central role of detachment faults in accretion of slow-spreading oceanic lithosphere. *Nature* **455**, 790–794 (2008).
50. Cannat, M. et al. Thin crust, ultramafic exposures, and rugged faulting patterns at the Mid-Atlantic Ridge (22°–24° N). *Geology* **23**, 49 (1995).
51. Tucholke, B. E., Lin, J. & Kleinrock, M. C. Megamullions and mullion structure defining oceanic metamorphic core complexes on the Mid-Atlantic Ridge. *J. Geophys. Res.* **103**, 9857–9866 (1998).
52. Karson, J. A. Internal structure of oceanic lithosphere: a perspective from tectonic windows. *Geophys. Monogr. Ser.* **106**, 177–218 (1998).
53. Cannat, M. et al. Spreading rate, spreading obliquity, and melt supply at the ultraslow spreading Southwest Indian Ridge. *Geochem. Geophys. Geosyst.* https://doi.org/10.1029/2007GC001676 (2008).
54. Escartín, J. et al. Tectonic structure, evolution, and the nature of oceanic core complexes and their detachment fault zones (13°20′N and 13° 30′N, Mid Atlantic Ridge). *Geochem. Geophys. Geosyst.* **18**, 1451–1482 (2017).
55. Smith, D. K., Escartín, J., Schouten, H. & Cann, J. R. Fault rotation and core complex formation: significant processes in seafloor formation at slow-spreading mid-ocean ridges (Mid-Atlantic Ridge, 13°–15°N). *Geochem. Geophys. Geosyst.* https://doi.org/10.1029/2007GC001699 (2008).
56. Cannat, M. et al. Modes of seafloor generation at a melt-poor ultraslow-spreading ridge. *Geology* **34**, 605–608 (2006).
57. Dick, H. J. B., Tivey, M. A. & Tucholke, B. E. Plutonic foundation of a slow-spreading ridge segment: oceanic core complex at Kane Megamullion, 23°30′N, 45°20′W. *Geochem. Geophys. Geosyst.* https://doi.org/10.1029/2007GC001645 (2008).
58. Sauter, D. et al. Continuous exhumation of mantle-derived rocks at the Southwest Indian Ridge for 11 million years. *Nat. Geosci.* **6**, 314–320 (2013).
59. Michael, P. J. et al. Magmatic and amagmatic seafloor generation at the ultraslow-spreading Gakkel ridge, Arctic Ocean. *Nature* **423**, 956–961 (2003).
60. MacLeod, C. J. et al. Life cycle of oceanic core complexes. *Earth Planet. Sci. Lett.* **287**, 333–344 (2009).
61. Schroeder, T. & John, B. E. Strain localization on an oceanic detachment fault system, Atlantis Massif, 30°N, Mid-Atlantic Ridge. *Geochem. Geophys. Geosyst.* https://doi.org/10.1029/2004GC000728 (2004).
62. Bickert, M., Lavier, L. & Cannat, M. How do detachment faults form at ultraslow mid-ocean ridges in a thick axial lithosphere? *Earth Planet. Sci. Lett.* **533**, 116048 (2020).
63. McCaig, A. M., Delacour, A., Fallick, A. E., Castelain, T. & Früh-Green, G. L. Detachment fault control on hydrothermal circulation systems: interpreting the subsurface beneath the TAG hydrothermal field using the isotopic and geological evolution of oceanic core complexes in the Atlantic. *Geophys. Monogr. Ser.* **188**, 207–239 (2010).
64. Boschi, C., Früh-Green, G. L., Delacour, A., Karson, J. A. & Kelley, D. S. Mass transfer and fluid flow during detachment faulting and development of an oceanic core complex, Atlantis Massif (MAR 30° N). *Geochem. Geophys. Geosyst.* https://doi.org/10.1029/2005GC001074. (2006).
65. Kelley, D. S. et al. A serpentinite-hosted ecosystem: the lost city hydrothermal field. *Science* **307**, 1428–1434 (2005).
66. Karson, J. A. et al. Detachment shear zone of the Atlantis Massif core complex, Mid-Atlantic Ridge, 30° N. *Geochem. Geophys. Geosyst.* https://doi.org/10.1029/2005GC001109 (2006).
67. Colaço, A. et al. MoMAR-D: a technological challenge to monitor the dynamics of the Lucky Strike vent ecosystem. *ICES J. Mar. Sci.* **68**, 416–424 (2011).
68. Barreyre, T. et al. Structure, temporal evolution, and heat flux estimates from the Lucky Strike deep-sea hydrothermal field derived from seafloor image mosaics. *Geochem. Geophys. Geosyst.* https://doi.org/10.1029/2011GC003990 (2012).
69. Mittelstaedt, E. et al. Quantifying diffuse and discrete venting at the Tour Eiffel vent site, Lucky Strike hydrothermal field. *Geochem. Geophys. Geosyst.* https://doi.org/10.1029/2011GC003991 (2012).
70. Lowell, R. P. et al. Magma-hydrothermal interactions at the Costa Rica Rift from data collected in 1994 and 2015. *Earth Planet. Sci. Lett.* **531**, 115991 (2020).
71. Fontaine, F. J., Cannat, M., Escartin, J. & Crawford, W. C. Along-axis hydrothermal flow at the axis of slow spreading Mid-Ocean Ridges: insights from numerical models of the Lucky Strike vent field (MAR). *Geochem. Geophys. Geosyst.* **15**, 2918–2931 (2014).
72. McCaig, A. M., Cliff, R. A., Escartin, J., Fallick, A. E. & MacLeod, C. J. Oceanic detachment faults focus very large volumes of black smoker fluids. *Geology* **35**, 935–938 (2007).
73. Kent, G. M., Harding, A. J. & Orcutt, J. A. Distribution of magma beneath the East Pacific Rise between the Clipperton Transform and the 9° 17′ N Deval from forward modeling of common depth point data. *J. Geophys. Res.* **98**, 13945–13969 (1993).
74. Canales, J. P. et al. Upper crustal structure and axial topography at intermediate spreading ridges: Seismic constraints from the southern Juan de Fuca Ridge. *J. Geophys. Res.* **110**, B12104 (2005).
75. Phipps Morgan, J. & Chen, Y. J. Dependence of ridge-axis morphology on magma supply and spreading rate. *Nature* **364**, 706–708 (1993).
76. deMartin, B. J., Sohn, R. A., Pablo Canales, J. & Humphris, S. E. Kinematics and geometry of active detachment faulting beneath the Trans-Atlantic Geotraverse (TAG) hydrothermal field on the Mid-Atlantic Ridge. *Geology* **35**, 711–714 (2007).
77. Cannat, M. Emplacement of mantle rocks in the seafloor at mid-ocean ridges. *J. Geophys. Res.* **98**, 4163–4172 (1993).
78. Wilcock, W. S. D. & Delaney, J. R. Mid-ocean ridge sulfide deposits: evidence for heat extraction from magma chambers or cracking fronts? *Earth Planet. Sci. Lett.* **145**, 49–64 (1996).
79. Kelley, D. S. & Shank, T. M. Hydrothermal systems: a decade of discovery in slow spreading environments. *Geophys. Monogr. Ser.* **188**, 369–407 (2010).
80. Kelley, D. S. et al. An off-axis hydrothermal vent field near the Mid-Atlantic Ridge at 30° N. *Nature* **412**, 145–149 (2001).
81. Lecoeuvre, A., Ménez, B., Cannat, M., Chavagnac, V. & Gérard, E. Microbial ecology of the newly discovered serpentinite-hosted Old City hydrothermal field (southwest Indian ridge). *ISME J.* **15**, 818–832 (2021).
82. Connelly, D. P. et al. Hydrothermal vent fields and chemosynthetic biota on the world's deepest seafloor spreading centre. *Nat. Commun.* **3**, 620 (2012).
83. German, C. R. et al. Diverse styles of submarine venting on the ultraslow spreading Mid-Cayman Rise. *Proc. Natl Acad. Sci. USA* **107**, 14020–14025 (2010).
84. McDermott, J. M., Seewald, J. S., German, C. R. & Sylva, S. P. Pathways for abiotic organic synthesis at submarine hydrothermal fields. *Proc. Natl Acad. Sci. USA* **112**, 7668–7672 (2015).
85. Hayman, N. W. et al. Oceanic core complex development at the ultraslow spreading Mid-Cayman Spreading Center. *Geochem. Geophys. Geosyst.* https://doi.org/10.1029/2010GC003240 (2011).
86. Barreyre, T., Parnell-Turner, R., Wu, J.-N. & Fornari, D. J. Tracking crustal permeability and hydrothermal response during seafloor eruptions at the East Pacific Rise, 9° 50′ N. *Geophys. Res. Lett.* e2021GL095459 (2022).
87. Alt, J. C. in *Seafloor Hydrothermal Systems: Physical, Chemical, Biological, and Geological Interactions* Vol. 91 (eds Humphris, S. E. et al.) 85–114 (American Geophysical Union, 1995).
88. Tivey, M. K. Generation of seafloor hydrothermal vent fluids and associated mineral deposits. *Oceanography* **20**, 50–65 (2007).
89. Butterfield, D. A. et al. Mixing, reaction and microbial activity in the sub-seafloor revealed by temporal and spatial variation in diffuse flow vents at Axial Volcano. *Geophys. Monogr. Ser.* **144**, 269–289 (2004).
90. Von Damm, K. L. & Lilley, M. D. Diffuse flow hydrothermal fluids from 9° 50′ N East Pacific Rise: origin, evolution and biogeochemical controls. *Geophys. Monogr. Ser.* **144**, 245–268 (2004).
91. Opatkiewicz, A. D., Butterfield, D. A. & Baross, J. A. Individual hydrothermal vents at Axial Seamount harbor distinct subseafloor microbial communities. *FEMS Microbiol. Ecol.* **70**, 413–424 (2009).
92. Fortunato, C. S., Larson, B., Butterfield, D. A. & Huber, J. A. Spatially distinct, temporally stable microbial populations mediate biogeochemical cycling at and below the seafloor in hydrothermal vent fluids: microbial genomics at axial seamount. *Environ. Microbiol.* **20**, 769–784 (2018).
93. Deming, J. W. & Baross, J. A. Deep-sea smokers: windows to a subsurface biosphere? *Geochim. Cosmochim. Acta* **57**, 3219–3230 (1993).
94. Huber, J. A. et al. Microbial population structures in the deep marine biosphere. *Science* **318**, 97–100 (2007).

95. Sogin, M. L. et al. Microbial diversity in the deep sea and the underexplored 'rare biosphere'. *Proc. Natl Acad. Sci. USA* **103**, 12115–12120 (2006).
96. Dick, G. J. The microbiomes of deep-sea hydrothermal vents: distributed globally, shaped locally. *Nat. Rev. Microbiol.* https://doi.org/10.1038/s41579-019-0160-2 (2019).
97. Bischoff, J. L. & Rosenbauer, R. J. An empirical equation of state for hydrothermal seawater (3.2 percent NaCl). *Am. J. Sci.* **285**, 725–763 (1985).
98. Kelley, D. S. & Delaney, J. R. Two-phase separation and fracturing in mid-ocean ridge gabbros at temperatures greater than 700°C. *Earth Planet. Sci. Lett.* **83**, 53–66 (1987).
99. Fournier, R. O. Conceptual models of brine evolution in magmatic-hydrothermal systems. *US Geol. Surv. Prof. Pap.* **1350**, 1487–1506 (1987).
100. Coumou, D., Driesner, T., Weis, P. & Heinrich, C. A. Phase separation, brine formation, and salinity variation at black smoker hydrothermal systems. *J. Geophys. Res.* **114**, B03212 (2009).
101. Chavagnac, V. et al. Spatial variations in vent chemistry at the lucky strike hydrothermal field, mid-atlantic ridge (37°N): updates for subseafloor flow geometry from the newly discovered Capelinhos Vent. *Geochem. Geophys. Geosyst.* **19**, 4444–4458 (2018).
102. Xu, G. & Lavelle, J. W. Circulation, hydrography, and transport over the summit of Axial seamount, a deep volcano in the Northeast Pacific. *J. Geophys. Res. Ocean.* **122**, 5404–5422 (2017).
103. Kaye, J. Z. & Baross, J. A. High incidence of halotolerant bacteria in Pacific hydrothermal-vent and pelagic environments. *FEMS Microbiol. Ecol.* **32**, 249–260 (2000).
104. Haase, K. M. et al. Young volcanism and related hydrothermal activity at 5° S on the slow-spreading southern Mid-Atlantic Ridge. *Geochem. Geophys. Geosyst.* https://doi.org/10.1029/2006GC001509 (2007).
105. Koschinsky, A. et al. Hydrothermal venting at pressure-temperature conditions above the critical point of seawater, 5° S on the Mid-Atlantic Ridge. *Geology* **36**, 615–618 (2008).
106. Pester, N. J., Ding, K. & Seyfried, W. E. Magmatic eruptions and iron volatility in deep-sea hydrothermal fluids. *Geology* **42**, 255–258 (2014).
107. Butterfield, D. A. et al. in *Mid-Ocean Ridges* (eds Cann, J.R., Elderfield, H. & Laughton, A.S.) 153–170 (Cambridge Univ. Press, 1999).
108. Von Damm, K. L. Chemistry of hydrothermal vent fluids from 9°–10° N, East Pacific Rise: 'Time zero,' the immediate posteruptive period. *Geophys. Res.* **105**, 11203–11222 (2000).
109. Von Damm, K. L. et al. Extraordinary phase separation and segregation in vent fluids from the southern East Pacific Rise. *Earth Planet. Sci. Lett.* **206**, 365–378 (2003).
110. Butterfield, D. A. et al. Seafloor eruptions and evolution of hydrothermal fluid chemistry. *Phil. Trans. R. Soc. Lond. A* **355**, 369–386 (1997).
111. Seewald, J., Cruse, A. & Saccocia, P. Aqueous volatiles in hydrothermal fluids from the Main Endeavour Field, northern Juan de Fuca Ridge: temporal variability following earthquake activity. *Earth Planet. Sci. Lett.* **216**, 575–590 (2003).
112. Love, B., Lilley, M., Butterfield, D., Olson, E. & Larson, B. Rapid variations in fluid chemistry constrain hydrothermal phase separation at the Main Endeavour Field. *Geochem. Geophys. Geosyst.* **18**, 531–543 (2017).
113. Rommevaux, C. et al. Prokaryote communities at active chimney and in situ colonization devices after a magmatic degassing event (37° N MAR, EMSO-Azores Deep-Sea Observatory). *Geochem. Geophys. Geosyst.* **20**, 3065–3089 (2019).
114. Baker, E. T., Massoth, G. J. & Feely, R. A. Cataclysmic hydrothermal venting on the Juan de Fuca Ridge. *Nature* **329**, 149–151 (1987).
115. Lupton, J. E., Baker, E. T. & Massoth, G. J. Helium, heat, and the generation of hydrothermal event plumes at mid-ocean ridges. *Earth Planet. Sci. Lett.* **171**, 343–350 (1999).
116. Holden, J. F., Summit, M. & Baross, J. A. Thermophilic and hyperthermophilic microorganisms in 3–30 °C hydrothermal fluids following a deep-sea volcanic eruption. *FEMS Microbiol. Ecol.* **25**, 33–41 (1998).
117. Summit, M. & Baross, J. A. Thermophilic subseafloor microorganisms from the 1996 North Gorda Ridge eruption. *Deep Sea Res. II Top. Stud. Oceanogr.* **45**, 2751–2766 (1998).
118. Kelley, D. S., Lilley, M. D., Lupton, J. E. & Olson, E. J. Enriched H_2, CH_4, and ^3He concentrations in hydrothermal plumes associated with the 1996 Gorda Ridge eruptive event. *Deep Sea Res. II Top. Stud. Oceanogr.* **45**, 2665–2682 (1998).
119. Spietz, R. et al. Deep-sea volcanic eruptions create unique chemical and biological linkages between the subsurface lithosphere and the oceanic hydrosphere. *Oceanography* **31**, 128–135 (2018).
120. Meyer, J. L., Akerman, N. H., Proskurowski, G. & Huber, J. A. Microbiological characterization of post-eruption "snowblower" vents at Axial Seamount, Juan de Fuca Ridge. *Front. Microbiol.* **4**, 153 (2013).
121. Gold, T. The deep, hot biosphere. *Proc. Natl Acad. Sci. USA* **89**, 6045–6049 (1992).
122. Baross, J. A. et al. in *The Subseafloor Biosphere at Mid-Ocean Ridges* Vol. 144 (eds Wilcock, W. S. D. et al.) 1–11 (American Geophysical Union, 2004).
123. Davis, E. E. & Fisher, A. T. in *Encyclopedia of Solid Earth Geophysics* (ed. Gupta, H. K.) https://doi.org/10.1007/978-3-030-10475-7_65-1 (Springer, 2020).
124. Simoneit, B. R. T., Kawka, O. E. & Brault, M. Origin of gases and condensates in the Guaymas Basin hydrothermal system (Gulf of California). *Chem. Geol.* **71**, 169–182 (1988).
125. Cruse, A. M. & Seewald, J. S. Geochemistry of low-molecular weight hydrocarbons in hydrothermal fluids from Middle Valley, northern Juan de Fuca Ridge. *Geochim. Cosmochim. Acta* **70**, 2073–2092 (2006).
126. Mottl, M. J. et al. Middle Valley, Juan de Fuca Ridge. *Proc. Ocean Drill. Prog. Sci. Results* **139** (1994).
127. Zierenberg, R. A., Fouquet, Y., Miller, D. J. & Normark, W. R. *Proc. Ocean Drill. Prog. Sci. Results* **169**, http://www-odp.tamu.edu/publications/169_SR/169TOC.HTM (2000).
128. Ishibashi, J. et al. Helium and carbon gas geochemistry of pore fluids from the sediment-rich hydrothermal system in Escanaba Trough. *Appl. Geochem.* **17**, 1457–1466 (2002).
129. Von Damm, K. L. et al. The Escanaba Trough, Gorda Ridge hydrothermal system: temporal stability and subseafloor complexity. *Geochim. Cosmochim. Acta* **69**, 4971–4984 (2005).
130. Teske, A. et al. The Guaymas Basin Hiking Guide to hydrothermal mounds, chimneys, and microbial mats: complex seafloor expressions of subsurface hydrothermal circulation. *Front. Microbiol.* https://doi.org/10.3389/fmicb.2016.00075 (2016).
131. Paduan, J. B. et al. Discovery of hydrothermal vent fields on Alarcón rise and in Southern Pescadero Basin, Gulf of California. *Geochem. Geophys. Geosyst.* **19**, 4788–4819 (2018).
132. Kawka, O. E. & Simoneit, B. R. T. Hydrothermal pyrolysis of organic matter in Guaymas Basin: I. Comparison of hydrocarbon distributions in subsurface sediments and seabed petroleums. *Org. Geochem.* **22**, 947–978 (1994).
133. Lilley, M. D. et al. Anomalous CH4 and NH4+ concentrations at an unsedimented mid-ocean-ridge hydrothermal system. *Nature* **364**, 45–47 (1993).
134. You, C.-F. et al. Boron and halide systematics in submarine hydrothermal systems: effects of phase separation and sedimentary contributions. *Earth Planet. Sci. Lett.* **123**, 227–238 (1994).
135. Proskurowski, G., Lilley, M. D. & Brown, T. A. Isotopic evidence of magmatism and seawater bicarbonate removal at the endeavour hydrothermal system. *Earth Planet. Sci. Lett.* **225**, 53–61 (2004).
136. Pedersen, R. B. et al. Discovery of a black smoker vent field and vent fauna at the Arctic Mid-Ocean Ridge. *Nat. Commun.* **1**, 126 (2010).
137. Baumberger, T. et al. Fluid composition of the sediment-influenced Loki's Castle vent field at the ultra-slow spreading Arctic Mid-Ocean Ridge. *Geochim. Cosmochim. Acta* **187**, 156–178 (2016).
138. Charlou, J. L. et al. High production and fluxes of H_2 and CH_4 and evidence of abiotic hydrocarbon synthesis by serpentinization in ultramafic-hosted hydrothermal systems on the Mid-Atlantic Ridge. *Geophys. Monogr. Ser.* **188**, 265–296 (2010).
139. Andreani, M. et al. Tectonic structure, lithology, and hydrothermal signature of the Rainbow massif (Mid-Atlantic Ridge 36°14′N). *Geochem. Geophys. Geosyst.* **15**, 3543–3571 (2014).
140. Charlou, J. L., Donval, J. P., Fouquet, Y., Jean-Baptiste, P. & Holm, N. Geochemistry of high H_2 and CH_4 vent fluids issuing from ultramafic rocks at the Rainbow hydrothermal field (36°14′N, MAR). *Chem. Geol.* **191**, 345–359 (2002).
141. Frost, B. R. On the stability of sulfides, oxides, and native metals in serpentinite. *J. Petrol.* **26**, 31–63 (1985).
142. Abrajano, T. A. et al. Methane-hydrogen gas seeps, Zambales ophiolite, Philippines: deep or shallow origin? *Chem. Geol.* **71**, 211–222 (1988).
143. McCollom, T. M., Klein, F., Solheid, P. & Moskowitz, B. The effect of pH on rates of reaction and hydrogen generation during serpentinization. *Phil. Trans. R. Soc. A.* **378**, 20180428 (2020).
144. McCollom, T. M. & Bach, W. Thermodynamic constraints on hydrogen generation during serpentinization of ultramafic rocks. *Geochim. Cosmochim. Acta* **73**, 856–875 (2009).
145. Martin, W. & Russell, M. J. On the origin of biochemistry at an alkaline hydrothermal vent. *Phil. Trans. R. Soc. B* **362**, 1887–1926 (2007).
146. Martin, W., Baross, J., Kelley, D. & Russell, M. J. Hydrothermal vents and the origin of life. *Nat. Rev. Microbiol.* **6**, 805–814 (2008).
147. Russell, M. J., Hall, A. J. & Martin, W. Serpentinization as a source of energy at the origin of life. *Geobiology* **8**, 355–371 (2010).
148. Hannington, M. D., De Ronde, C. E. J. & Petersen, S. in *Economic Geology One Hundredth Anniversary Volume* https://doi.org/10.5382/AV100.06 (Society of Economic Geologists, 2005).
149. Schmidt, K., Koschinsky, A., Garbe-Schönberg, D., de Carvalho, L. M. & Seifert, R. Geochemistry of hydrothermal fluids from the ultramafic-hosted Logatchev hydrothermal field, 15° N on the Mid-Atlantic Ridge: temporal and spatial investigation. *Chem. Geol.* **242**, 1–21 (2007).
150. German, C. R. & Seyfried, W. E. in *Treatise on Geochemistry* 2nd edn, Vol. 8 (eds Holland, H. D. & Turekian, K. K.) 191–233 (Elsevier, 2014).
151. Seyfried, W. E., Pester, N. J., Ding, K. & Rough, M. Vent fluid chemistry of the Rainbow hydrothermal system (36° N, MAR): phase equilibria and in situ pH controls on subseafloor alteration processes. *Geochim. Cosmochim. Acta* **75**, 1574–1593 (2011).
152. Konn, C. et al. Extending the dataset of fluid geochemistry of the Menez Gwen, Lucky Strike, Rainbow, TAG and Snake Pit hydrothermal vent fields: investigation of temporal stability and organic contribution. *Deep. Sea Res. I Oceanogr. Res. Pap.* **179**, 103630 (2022).
153. Thurnherr, A. M. & Richards, K. J. Hydrography and high-temperature heat flux of the Rainbow hydrothermal site (36°14′N, Mid-Atlantic Ridge). *J. Geophys. Res.* **106**, 9411–9426 (2001).
154. Canales, J. P., Dunn, R. A., Arai, R. & Sohn, R. A. Seismic imaging of magma sills beneath an ultramafic-hosted hydrothermal system. *Geology* **45**, 451–454 (2017).
155. Früh-Green, G. L. et al. Magmatism, serpentinization and life: Insights through drilling the Atlantis Massif (IODP Expedition 357). *Lithos* **323**, 137–155 (2018).
156. Proskurowski, G. et al. Abiogenic hydrocarbon production at Lost City hydrothermal field. *Science* **319**, 604–607 (2008).
157. Lang, S. Q., Butterfield, D. A., Schulte, M., Kelley, D. S. & Lilley, M. D. Elevated concentrations of formate, acetate and dissolved organic carbon found at the Lost City hydrothermal field. *Geochim. Cosmochim. Acta* **74**, 941–952 (2010).

158. Proskurowski, G., Lilley, M. D., Kelley, D. S. & Olson, E. J. Low temperature volatile production at the Lost City hydrothermal field, evidence from a hydrogen stable isotope geothermometer. *Chem. Geol.* **229**, 331–343 (2006).
159. Früh-Green, G. L. et al. 30,000 years of hydrothermal activity at the Lost City vent field. *Science* **301**, 495–498 (2003).
160. Lang, S. Q. et al. Extensive decentralized hydrogen export from the Atlantis Massif. *Geology* **49**, 851–856 (2021).
161. Larson, B. I. et al. Stealth export of hydrogen and methane from a low temperature serpentinization system. *Deep. Sea Res. II Topical Stud. Oceanogr.* **121**, 233–245 (2015).
162. Ternieten, L., Früh-Green, G. L. & Bernasconi, S. M. Carbonate mineralogy in mantle peridotites of the Atlantis Massif (IODP Expedition 357). *J. Geophys. Res. Solid Earth* **126**, e2021JB021885 (2021).
163. Ternieten, L., Früh-Green, G. L. & Bernasconi, S. M. Distribution and sources of carbon in serpentinized mantle peridotites at the Atlantis Massif (IODP Expedition 357). *JGR Solid Earth* **126**, e2021JB021973 (2021).
164. Kelemen, P. B. & Matter, J. In situ carbonation of peridotite for CO_2 storage. *Proc. Natl Acad. Sci. USA* **105**, 17295–17300 (2008).
165. Moore, W. S., Frankle, J. D., Benitez-Nelson, C. R., Früh-Green, G. L. & Lang, S. Q. Activities of ^{223}Ra and ^{226}Ra in fluids from the Lost City hydrothermal field require short fluid residence times. *JGR Ocean.* **126**, e2021JC017886 (2021).
166. Kadko, D., Gronvold, K. & Butterfield, D. Application of radium isotopes to determine crustal residence times of hydrothermal fluids from two sites on the Reykjanes Peninsula, Iceland. *Geochim. Cosmochim. Acta* **71**, 6019–6029 (2007).
167. Kadko, D. & Butterfield, D. A. The relationship of hydrothermal fluid composition and crustal residence time to maturity of vent fields on the Juan de Fuca Ridge. *Geochim. Cosmochim. Acta* **62**, 1521–1533 (1998).
168. Reeves, E. P. Timing Earth's abiotic kitchen: short hydrothermal fluid residence times in serpentinizing oceanic crust. *JGR Oceans* **127**, e2022JC018601 (2022).
169. Klein, F., Grozeva, N. G. & Seewald, J. S. Abiotic methane synthesis and serpentinization in olivine-hosted fluid inclusions. *Proc. Natl Acad. Sci. USA* **116**, 17666–17672 (2019).
170. Etiope, G. & Whiticar, M. J. Abiotic methane in continental ultramafic rock systems: towards a genetic model. *Appl. Geochem.* **102**, 139–152 (2019).
171. McCollom, T. M. & Seewald, J. S. Abiotic synthesis of organic compounds in deep-sea hydrothermal environments. *Chem. Rev.* **107**, 382–401 (2007).
172. Kelley, D. S. & Früh-Green, G. L. Abiogenic methane in deep-seated mid-ocean ridge environments: insights from stable isotope analyses. *J. Geophys. Res.* **104**, 10439–10460 (1999).
173. Kelley, D. S. & Früh-Green, G. L. Volatile lines of descent in submarine plutonic environments: insights from stable isotope and fluid inclusion analyses. *Geochim. Cosmochim. Acta* **65**, 3325–3346 (2001).
174. Labidi, J. et al. Methane thermometry in deep-sea hydrothermal systems: evidence for re-ordering of doubly-substituted isotopologues during fluid cooling. *Geochim. Cosmochim. Acta* **288**, 248–261 (2020).
175. Wang, D. T., Reeves, E. P., McDermott, J. M., Seewald, J. S. & Ono, S. Clumped isotopologue constraints on the origin of methane at seafloor hot springs. *Geochim. Cosmochim. Acta* **223**, 141–158 (2018).
176. Amend, J. P., McCollom, T. M., Hentscher, M. & Bach, W. Catabolic and anabolic energy for chemolithoautotrophs in deep-sea hydrothermal systems hosted in different rock types. *Geochim. Cosmochim. Acta* **75**, 5736–5748 (2011).
177. Lang, S. Q. et al. Deeply-sourced formate fuels sulfate reducers but not methanogens at Lost City hydrothermal field. *Sci. Rep.* **8**, 755 (2018).
178. Lang, S. Q. & Brazelton, W. J. Habitability of the marine serpentinite subsurface: a case study of the Lost City hydrothermal field. *Phil. Trans. R. Soc. A* **378**, 20180429 (2020).
179. Schrenk, M. O., Kelley, D. S., Bolton, S. A. & Baross, J. A. Low archaeal diversity linked to subseafloor geochemical processes at the Lost City hydrothermal field, Mid-Atlantic Ridge. *Environ. Microbiol.* **6**, 1086–1095 (2004).
180. Adam, N. & Perner, M. Microbially mediated hydrogen cycling in deep-sea hydrothermal vents. *Front. Microbiol.* **9**, 1–17 (2018).
181. Mehta, M. P. & Baross, J. A. Nitrogen fixation at 92°C by a hydrothermal vent Archaeon. *Science* **314**, 1783–1786 (2006).
182. Brandes, J. A. et al. Abiotic nitrogen reduction on the early Earth. *Nature* **395**, 365–367 (1998).
183. Ménez, B. et al. Abiotic synthesis of amino acids in the recesses of the oceanic lithosphere. *Nature* **564**, 59–63 (2018).
184. Dasgupta, P. *The Economics of Biodiversity: The Dasgupta Review: Full Report* (HM Treasury, 2021).
185. Anderson, R. E. et al. Genomic variation in microbial populations inhabiting the marine subseafloor at deep-sea hydrothermal vents. *Nat. Commun.* **8**, 1114 (2017).
186. Poli, A. et al. Microbial diversity in extreme marine habitats and their biomolecules. *Microorganisms* **5**, 25 (2017).
187. Zeng, X., Alain, K. & Shao, Z. Microorganisms from deep-sea hydrothermal vents. *Mar. Life Sci. Technol.* **3**, 204–230 (2021).
188. Cathalot, C. et al. Hydrothermal plumes as hotspots for deep-ocean heterotrophic microbial biomass production. *Nat. Commun.* **12**, 6861 (2021).
189. Anderson, R. E. Tracking microbial evolution in the subseafloor biosphere. *mSystems* https://doi.org/10.1128/mSystems.00731-21 (2021).
190. Spang, A. et al. Complex archaea that bridge the gap between prokaryotes and eukaryotes. *Nature* **521**, 173–179 (2015).
191. Eme, L., Spang, A., Lombard, J., Stairs, C. W. & Ettema, T. J. G. Archaea and the origin of eukaryotes. *Nat. Rev. Microbiol.* **15**, 711–723 (2017).
192. Schleper, C. & Sousa, F. L. Meet the relatives of our cellular ancestor. *Nature* **577**, 478–479 (2020).
193. Williams, T. A., Cox, C. J., Foster, P. G., Szöllősi, G. J. & Embley, T. M. Phylogenomics provides robust support for a two-domains tree of life. *Nat. Ecol. Evol.* **4**, 138–147 (2020).
194. McNichol, J. et al. Primary productivity below the seafloor at deep-sea hot springs. *Proc. Natl Acad. Sci. USA* **115**, 6756–6761 (2018).
195. Thomas, E., Anderson, R. E., Li, V., Rogan, L. J. & Huber, J. A. Diverse viruses in deep-sea hydrothermal vent fluids have restricted dispersal across ocean basins. *mSystems* **6**, https://doi.org/10.1128/mSystems.00068-21 (2021).
196. Hu, S. K. et al. Protistan grazing impacts microbial communities and carbon cycling at deep-sea hydrothermal vents. *Proc. Natl Acad. Sci. USA* **118**, e2102674118 (2021).
197. Brazelton, W. J., Schrenk, M. O., Kelley, D. S. & Baross, J. A. Methane- and sulfur-metabolizing microbial communities dominate the Lost City hydrothermal field ecosystem. *Appl. Environ. Microbiol.* **72**, 6257–6270 (2006).
198. Brazelton, W. J. et al. Archaea and bacteria with surprising microdiversity show shifts in dominance over 1000-year time scales in hydrothermal chimneys. *Proc. Natl Acad. Sci. USA* **107**, 1612–1617 (2010).
199. Baross, J. A. & members of the Ocean Memory Project. The ocean carries 'memories' of SARS-CoV-2: We've been looking in the wrong place for a deeper understanding of the virus. *Sci. Am.* https://www.scientificamerican.com/article/the-ocean-carries-memories-of-sars-cov-2/ (2020).
200. Brazelton, W. J. & Baross, J. A. Abundant transposases encoded by the metagenome of a hydrothermal chimney biofilm. *ISME J.* **3**, 1420–1424 (2009).
201. Brazelton, W. J., Mehta, M. P., Kelley, D. S. & Baross, J. A. Physiological differentiation within a single-species biofilm fueled by serpentinization. *mBio* **2**, https://doi.org/10.1128/mBio.00127-11 (2011).
202. Kodolányi, J., Pettke, T., Spandler, C., Kamber, B. S. & Gméling, K. Geochemistry of ocean floor and fore-arc serpentinites: constraints on the ultramafic input to subduction zones. *J. Petrol.* **53**, 235–270 (2012).
203. Elderfield, H. & Schultz, A. Mid-ocean ridge hydrothermal fluxes and the chemical composition of the ocean. *Annu. Rev. Earth Planet. Sci.* **24**, 191–224 (1996).
204. Cannat, M., Cann, J. & Maclennan, J. Some hard rock constraints on the supply of heat to mid-ocean ridges. *Geophys. Monogr. Ser.* **148**, 111–149 (2004).
205. Coogan, L. A. & Dosso, S. An internally consistent, probabilistic, determination of ridge-axis hydrothermal fluxes from basalt-hosted systems. *Earth Planet. Sci. Lett.* **323–324**, 92–101 (2012).
206. Drever, J. I. The magnesium problem. *Mar. Chem.* **5**, 337 (1974).
207. Edmond, J. M. et al. Ridge crest hydrothermal activity and the balances of the major and minor elements in the ocean: the Galapagos data. *Earth Planet. Sci. Lett.* **46**, 1–18 (1979).
208. Shalev, N., Bontognali, T. R. R., Wheat, C. G. & Vance, D. New isotope constraints on the Mg oceanic budget point to cryptic modern dolomite formation. *Nat. Commun.* **10**, 5646 (2019).
209. Luther, G. W. Hydrothermal vents are a source of old refractory organic carbon to the deep ocean. *Geophys. Res. Lett.* **48**, e2021GL094869 (2021).
210. Hansell, D. A. Recalcitrant dissolved organic carbon fractions. *Annu. Rev. Mar. Sci.* **5**, 421–445 (2013).
211. Druffel, E. R. M., Williams, P. M., Bauer, J. E. & Ertel, J. R. Cycling of dissolved and particulate organic matter in the open ocean. *J. Geophys. Res.* **97**, 15639 (1992).
212. Lang, S. Q., Butterfield, D. A., Lilley, M. D., Paul Johnson, H. & Hedges, J. I. Dissolved organic carbon in ridge-axis and ridge-flank hydrothermal systems. *Geochim. Cosmochim. Acta* **70**, 3830–3842 (2006).
213. Hawkes, J. A. et al. Efficient removal of recalcitrant deep-ocean dissolved organic matter during hydrothermal circulation. *Nat. Geosci.* **8**, 856–860 (2015).
214. McCarthy, M. D. et al. Chemosynthetic origin of ^{14}C-depleted dissolved organic matter in a ridge-flank hydrothermal system. *Nat. Geosci.* **4**, 32–36 (2011).
215. Lin, H.-T., Repeta, D. J., Xu, L. & Rappé, M. S. Dissolved organic carbon in basalt-hosted deep subseafloor fluids of the Juan de Fuca Ridge flank. *Earth Planet. Sci. Lett.* **513**, 156–165 (2019).
216. Shah Walter, S. R. et al. Microbial decomposition of marine dissolved organic matter in cool oceanic crust. *Nat. Geosci.* **11**, 334–339 (2018).
217. Druffel, E. R. M. et al. Dissolved organic radiocarbon in the Eastern Pacific and Southern Oceans. *Geophys. Res. Lett.* **48**, e2021GL092904 (2021).
218. Früh-Green, G. L., Connolly, J. A. D., Plas, A., Kelley, D. S. & Grobéty, B. Serpentinization of oceanic peridotites: implications for geochemical cycles and biological activity. *Geophys. Monogr. Ser.* **144**, 119–136 (2004).
219. Delacour, A., Früh-Green, G. L., Bernasconi, S. M., Schaeffer, P. & Kelley, D. S. Carbon geochemistry of serpentinites in the Lost City hydrothermal system (30°N, MAR). *Geochim. Cosmochim. Acta* **72**, 3681–3702 (2008).
220. Resing, J. A. et al. Basin-scale transport of hydrothermal dissolved metals across the South Pacific Ocean. *Nature* **523**, 200–203 (2015).
221. Lough, A. J. M. et al. Diffuse hydrothermal venting: a hidden source of iron to the oceans. *Front. Mar. Sci.* https://doi.org/10.3389/fmars.2019.00329 (2019).
222. Ardyna, M. et al. Hydrothermal vents trigger massive phytoplankton blooms in the Southern Ocean. *Nat. Commun.* **10**, 2451 (2019).
223. Schine, C. M. S. et al. Massive Southern Ocean phytoplankton bloom fed by iron of possible hydrothermal origin. *Nat. Commun.* **12**, 1211 (2021).

224. Kleint, C. et al. Trace metal dynamics in shallow hydrothermal plumes at the Kermadec Arc. *Front. Mar. Sci.* **8**, 782734 (2022).
225. Guieu, C. et al. Iron from a submarine source impacts the productive layer of the Western Tropical South Pacific (WTSP). *Sci. Rep.* **8**, 9075 (2018).
226. Reese, B. K., Sobol, M. S., Bowles, M. W. & Hinrichs, K.-U. Redefining the subsurface biosphere: characterization of fungi isolated from energy-limited marine deep subsurface sediment. *Front. Fung. Biol.* https://doi.org/10.3389/ffunb.2021.727543 (2021).
227. Longnecker, K., Sievert, S. M., Sylva, S. P., Seewald, J. S. & Kujawinski, E. B. Dissolved organic carbon compounds in deep-sea hydrothermal vent fluids from the East Pacific Rise at 9°50′N. *Org. Geochem.* **125**, 41–49 (2018).
228. Grandy, J. J., Onat, B., Tunnicliffe, V., Butterfield, D. A. & Pawliszyn, J. Unique solid phase microextraction sampler reveals distinctive biogeochemical profiles among various deep-sea hydrothermal vents. *Sci. Rep.* **10**, 1360 (2020).
229. Noowong, A. et al. Imprint of Kairei and Pelagia deep-sea hydrothermal systems (Indian Ocean) on marine dissolved organic matter. *Org. Geochem.* **152**, 104141 (2021).
230. Sert, M. F. et al. Compositions of dissolved organic matter in the ice-covered waters above the Aurora hydrothermal vent system, Gakkel Ridge, Arctic Ocean. *Biogeosciences* **19**, 2101–2120 (2022).
231. Kelley, D. S., Delaney, J. R. & Juniper, S. K. Establishing a new era of submarine volcanic observatories: cabling axial seamount and the Endeavour Segment of the Juan de Fuca Ridge. *Mar. Geol.* **352**, 426–450 (2014).
232. Delaney, J. et al. Project NEPTUNE: an interactive, regional cabled ocean observatory in the northeast Pacific. *Proc. IEEE Oceans* https://doi.org/10.1109/OCEANS.2003.178480 (2003).
233. Delaney, J. R. & Barga, R. S. *Observing the Oceans — A 2020 Vision for Ocean Science* (Microsoft Research, 2009).
234. Petersen, S. et al. The geological setting of the ultramafic-hosted Logatchev hydrothermal field (14° 45′N, Mid-Atlantic Ridge) and its influence on massive sulfide formation. *Lithos* **112**, 40–56 (2009).
235. Bach, W. & Früh-Green, G. L. Alteration of the oceanic lithosphere and implications for seafloor processes. *Elements* **6**, 173–178 (2010).
236. Boetius, A. Lost city life. *Science* **307**, 1420–1422 (2005).
237. Rouméjon, S., Cannat, M., Agrinier, P., Godard, M. & Andreani, M. Serpentinization and fluid pathways in tectonically exhumed peridotites from the Southwest Indian Ridge (62–65° E). *J. Petrol.* **56**, 703–734 (2015).
238. Rouméjon, S., Früh-Green, G. L. & Orcutt, B. N. and the IODP Expedition 357 Science Party. Alteration heterogeneities in peridotites exhumed on the southern wall of the Atlantis Massif (IODP Expedition 357). *J. Petrol.* **59**, 1329–1358 (2018).
239. Hentscher, M. & Bach, W. Geochemically induced shifts in catabolic energy yields explain past ecological changes of diffuse vents in the East Pacific Rise 9°50′N area. *Geochem. Trans.* **13**, 2 (2012).
240. Kelley, D. S., Delaney, J. R. & Team, C. A. NSF's Cabled Array: a wired tectonic plate and overlying ocean. In *OCEANS 2016 MTS/IEEE Monterey* https://doi.org/10.1109/OCEANS.2016.7761398 (IEEE, 2016).
241. Nooner, S. L. & Chadwick, W. W. Inflation-predictable behavior and co-eruption deformation at Axial Seamount. *Science* **354**, 1399–1403 (2016).
242. Wilcock, W. S. D. et al. Seismic constraints on caldera dynamics from the 2015 Axial Seamount eruption. *Science* **354**, 1395–1399 (2016).
243. Barreyre, T. et al. Temporal variability and tidal modulation of hydrothermal exit-fluid temperatures at the Lucky Strike deep-sea vent field, Mid-Atlantic Ridge. *J. Geophys. Res. Solid. Earth* **119**, 2543–2566 (2014).
244. Barreyre, T. & Sohn, R. A. Poroelastic response of mid-ocean ridge hydrothermal systems to ocean tidal loading: Implications for shallow permeability structure. *Geophys. Res. Lett.* **43**, 1660–1668 (2016).
245. Bohidar, S., Crawford, W. C. & Cannat, M. Temporal and spatial evolution of seismicity at Lucky Strike volcano, Mid-Atlantic Ridge. AGU Abstract V35A-0122 (American Geophysical Union, 2021).
246. Miller, D. J. & Iturrino, G. J. & Christensen. Geochemical and petrological constraints on velocity behavior of lower crustal and upper mantle rocks from the fast-spreading ridge at Hess Deep. *Proc. Ocean. Drill. Prog. Sci. Results* **147**, 477–490 (1996).
247. Hirth, G., Escartín, J. & Lin, J. The rheology of the lower oceanic crust: implications for lithospheric deformation at mid-ocean ridges. *Geophys. Monogr. Ser.* **106**, 291–303 (1998).
248. Boschi, C., Dini, A., Früh-Green, G. L. & Kelley, D. S. Isotopic and element exchange during serpentinization and metasomatism at the Atlantis Massif (MAR 30° N): insights from B and Sr isotope data. *Geochim. Cosmochim. Acta* **72**, 1801–1823 (2008).
249. Alt, J. C. & Shanks, W. C. Serpentinization of abyssal peridotites from the MARK area, Mid-Atlantic Ridge: sulfur geochemistry and reaction modeling. *Geochim. Cosmochim. Acta* **67**, 641–653 (2003).
250. Andreani, M., Muñoz, M., Marcaillou, C. & Delacour, A. μXANES study of iron redox state in serpentine during oceanic serpentinization. *Lithos* **178**, 70–83 (2013).
251. Mayhew, L. E. & Ellison, E. T. A synthesis and meta-analysis of the Fe chemistry of serpentinites and serpentine minerals. *Phil. Trans. R. Soc. A* **378**, 20180420 (2020).

Acknowledgements

G.L.F.-G. acknowledges support from the Swiss National Science Foundation (grant no. 200021-163187). Support to D.S.K. was provided by the US National Science Foundation grant no. OCE-0137206, the Management and Operation of the Ocean Observatories Initiative grant 1743430 and the University of Washington. M.D.L. was supported by the US National Science Foundation (grants OCE-1037874 and 535962) and the W.M. Keck Foundation for Project NEPTUNE. The authors acknowledge the late Karen L. Von Damm, who pioneered and inspired decades of MOR hydrothermal vent research discussed in this Review. We further acknowledge the unwaning efforts of John R. Delaney, who was instrumental in driving the innovative ideas behind installing seafloor observatories at JdF.

Author contributions

G.L.F.-G. coordinated and led the writing of this Review. M.D.L. contributed to all aspects of writing, compiled data and led discussions on hydrothermal vent discoveries, distributions, fluid chemistry, volatiles and fluxes. D.S.K. led discussions on Axial, Endeavour, Ocean Observatories, phase separation and water–rock–microbe interactions, and together with her CEV team provided many of the figures. M.C. and V.C. provided input on slow- and ultraslow-spreading ridges and the EMSO observatory. J.A.B. wrote all sections on life in hydrothermal environments. All authors participated in discussions and edited multiple versions of the manuscript.

Competing interests

The authors declare no competing interests.

Additional information

Supplementary information The online version contains supplementary material available at https://doi.org/10.1038/s43017-022-00364-y.

Correspondence should be addressed to Gretchen L. Früh-Green.

Peer review information *Nature Reviews Earth & Environment* thanks W. Bach, S. Sievert and the other, anonymous, reviewer(s) for their contribution to the peer review of this work.

Related links

European Multidisciplinary Seafloor and water-column Observatory (EMSO): https://www.emso-fr.org/EMSO-Azores
MARUM: https://www.marum.de/en/Discover/Deep-Sea.html
Ocean Networks Canada: https://www.oceannetworks.ca/observatories/
Ocean Observatories Initiative (OOI) Regional Cabled Array: https://interactiveoceans.washington.edu
WHOI: https://www.whoi.edu

[1]Department of Earth Sciences, ETH Zurich, Zurich, Switzerland. [2]School of Oceanography, University of Washington, Seattle, Washington, USA. [3]Équipe de Géosciences Marines, Université de Paris, Institut de Physique du Globe de Paris, UMR CNRS, Paris, France. [4]Géosciences Environnement Toulouse, Université de Toulouse, UMR CNRS, Toulouse, France.